INTERACTION OF GAS BUBBLES WITH LIQUID LEAD

A Thesis Submitted
In Partial Fulfilment of the Requirements
FOR THE DEGREE OF
MASTER OF TECHNOLOGY

BY
ANWAR ALI

DEPARTMENT OF METALLURGICAL ENGINEERING
INDIAN INSTITUTE OF TECHNOLOGY KANPUR
JANUARY, 1973

V
JUNE '76

A 23389
29 MAR 1973

Theses
G69.4
AC 41

ME-1973-M-ALI-INT

POST GRADUATE OFFICE
17
Sub... 4.73.

CERTIFICATE

Certified that this work on 'Interaction of Gas Bubbles with Liquid Lead' has been carried out under my supervision and that it has not been submitted elsewhere for a degree.

H.S. RAY
Assistant Professor
Department of Metallurgical Engineering
Indian Institute of Technology, Kanpur.

POST GRADUATE OFFICE
This thesis has been approved for the award of ... Tech.)
in accordance with the regulations of the Indian Institute of Technology, Kanpur
Dated. 13.2.73

ACKNOWLEDGEMENTS

The author is deeply grateful to Dr. H.S. Ray for his valuable guidance and constant encouragement throughout the work.

The author also takes this opportunity to express his gratitude to Mr. Chandan Roy for the selfless help he gave throughout the work.

He also wishes to thank Dr. K.P. Jagannathan, Dr. S. Basu and Mr. S. Mazumdar for their help and useful suggestions. And finally, the author thanks Mr. M. Natu for his excellent typing.

TABLE OF CONTENTS

		Page
	LIST OF TABLES	v
	LIST OF FIGURES	vi
	LIST OF SYMBOLS	vii
	ABSTRACT	x
Chapter 1	INTRODUCTION	1
Chapter 2	LITERATURE SURVEY	4
2.0	Introduction	4
2.1	Studies on low temperature liquids	4
2.2	Studies on bubble-liquid metal interaction	11
2.3	Use of a solid electrolyte cell for kinetic measurements	18
Chapter 3	APPARATUS AND EXPERIMENTAL PROCEDURE	21
3.1	The furnace and the power supply arrangement	21
3.2	The gas purification train	23
3.3	Arrangement for control of gas composition and measurement of gas flow rates.	23
3.4	The e.m.f. measuring and recording devices.	25
3.5	The cell assembly	25
3.6	Experimental procedure	28
Chapter 4	RESULTS AND DISCUSSION	31
4.1	Theoretical background	31
4.2	Results and discussion	38
Chapter 5	CONCLUSIONS	72
Chapter 6	SUGGESTIONS FOR FURTHER STUDIES	73
	LIST OF REFERENCES	74

LIST OF TABLES

		Page
Table 1 -	Systems purified by oxygen or chlorine bubbling	2
Tables 2 - 5	Hydrogen reduction of oxygen saturated lead	40-46
Tables 6-10	Oxidation of liquid lead by argon-oxygen mixture	54-58
Table 11	Calculated values of mass transfer coefficients, K_L, across bubble-metal interface, and D/δ, across the free surface and values of boundary layer thickness δ.	67
Table 12	Comparison of observed values of K_L with theoretical values.	71

LIST OF FIGURES

		Page
Fig. 1	Schematic diagram of the power supply unit.	22
Fig. 2	Schematic diagram of the gas purification train.	24
Fig. 3	Gas mixer flow measuring system	26
Fig. 4	Cell assembly	27
Figs. 5,6,7 and 8	Plots of log C vs. time for hydrogen reduction runs	47-50
Figs. 9, 10	Plots of slopes of log(C) vs. time plots versus flow rate for hydrogen reduction.	52,53
Figs. 11-15	Plots of log (C_s-C) vs. time for oxidation runs.	59-63
Figs. 16,17	Plots of slopes of log (C_s-C) vs. time plots versus flow rate for oxidation.	65,66
Fig. 18	Plot of K_L vs. equivalent bubble radius	69
Fig. 19	Plot of log K_L vs. 1/T	70

LIST OF SYMBOLS

Roman Alphabets

a = Semi-major axis of oblate spheroidal bubble.

a_b = Area of bubble-metal interface

a_1 = Constant

A_b = Total instantaneous area of spherical bubbles

A_s = Area of the top surface of the melt.

A_{c-c} = Total instantaneous area of spherical-cap bubbles.

A_{os} = Surface area of oblate spheroidal bubble.

b_1, b_2 = Constants

C = Concentration of oxygen in the bulk of the metal at any time.

C_s = Concentration of oxygen at the bubble-metal interface.

C_o = Initial concentration of oxygen in the bulk of the metal.

d = Diameter of the container vessel.

d_b = Diameter of a sphere having volume equivalent to that of the bubble (equivalent diameter of the bubble).

d_o = Diameter of the orifice through which the bubble comes out.

D = Diffusion coefficient of solute in liquid.

E = Eccentricity of oblate spheroidal bubble

F = Flow rate of gas

F_D = Drag force exerted by liquid on bubble.

g = Acceleration due to gravity.

h = Height of rise of the bubble.

K_L = Mass transfer coefficient of solute in liquid.

n = Number of bubbles in liquid at any time.

n_C = Number of moles of oxygen removed (or dissolved).

N_{Re} = Reynolds number ($\frac{\rho d_b U}{\mu}$)

N_{Sc} = Schmidt number ($\frac{\mu}{\rho D}$)

N_{Sh} = Sherwood number ($\frac{K_L d_b}{D}$)

N_{Re_j} = Jet Reynolds number ($\frac{\rho' d_o U_t}{\mu}$)

p = Pressure in the top space above melt.

p_i = Initial pressure in top space.

P = Pressure in the bubble.

q = Sievert's law constant.

r_b = Equivalent radius of the bubble.

r_c = Radius of curvature of spherical surface of spherical-cap.bubble.

R = Universal gas constant.

S = Shape factor

t = Time

T = Temperature

U = Terminal velocity of bubble in real medium.

U_∞ = Terminal velocity of bubble in medium of infinite width.

U_t = Velocity of gas in jet.

v = Volume of top space above melt.

V = Volume of bubble

V_m = Volume of melt

Greek Alphabets

δ = Boundary layer thickness

μ = Viscosity of liquid

μ' = Viscosity of gas

ρ = Density of liquid

ρ' = Density of gas

σ = Surface tension of liquid

τ_r = Time of residence of bubble in liquid.

ABSTRACT

Name of student : Anwar Ali

Programme : M.Tech.

Department : Metallurgical Engineering

Title of Thesis : Interaction of gas bubbles with liquid lead.

Thesis Supervisor: Dr. H.S. Ray.

An electromotive force cell, employing the ZrO_2-CaO solid electrolyte, has been used to investigate the kinetics of oxidation of liquid lead, when a mixture of argon and oxygen is being bubbled through it, and the kinetics of its reduction during hydrogen bubbling. The solid electrolyte cell is of the type

Ni , NiO | ZrO_2 + CaO | Pb , O

(molten lead) solid electrolyte

Reference electrode — Oxygen diaphragm — Indicator electrode

The bubbling of either the oxidising or the reducing gas through the liquid lead is achieved by means of a stainless steel tube dipped in the lead melt. By changing the orifice diameter of the steel tube the diameter of the bubble emanating from the tube can be changed.

The changing concentration of oxygen in the liquid lead during either oxidation or reduction results in a constantly changing e.m.f. of the cell and this e.m.f. is continuously recorded.

During both oxidation and reduction the rate of dissolution or removal of oxygen is observed to increase initially, attain a constant value and then decrease at the end of each run. The rate of both oxidation and reduction is observed to be the fastest for the smallest bubble size and the largest flow rate.

CHAPTER 1

INTRODUCTION

The interaction of gas bubbles with liquid metals is of considerable importance in some refining reactions in process metallurgy. In the pyrometallurgical extraction of metals from ores, many of the impurities present as associated minerals in the ore remain with the metal. Such impurities may not be desirable and may have to be removed either chemically or physically.

Chemical refining consists of introducing into the basis metal, a reagent which combines with one or more of the impurities to form compounds which are insoluble in the metal. Oxygen is frequently used as a refining reagent and usually a flux is added to remove the oxide impurities in liquid form. Chlorine also serves as a refining agent for removing impurities from some metals. The passing of bubbles through an impure metal provides a quick means of removing the impurities. The bubbles provide a large area of contact with the metal and at the same time cause agitation in the bath, thus enhancing the rate of removal of the impurities.

Table 1 lists some systems which may be purified by bubbling oxygen or chlorine.

Gaseous impurities in metals may also be removed by bubbling a gas which has low solubility in the metal.

Table 1

Systems purified by oxygen or chlorine bubbling

Liquid metal	Impurities removed by oxygen bubbling	Impurities removed by chlorine bubbling
Iron	C, Si, P, Mn	Zn
Copper	Pb, As, Sb, S, Mg, Al, Fe	Fe, Pb, Zn
Lead	As, Sb, Sn, Zn	-
Zinc	Na	Pb
Bismuth	Pb, As, Sn, Zn	-
Tin	Fe, Al, Zn, Ni	-
Silver	Pb, Zn, Cu	-
Gold	Zn	Ag, Pb, Cu, Sb
Aluminium	-	Mg
Nickel	-	Cu

The mechanism of removal of the impurities is, however, not well understood in the sense that it might be either one of the following:- i) migration of the impurities to the bubbles of the refining gas and subsequent reaction at the gas metal interface or ii) initial dissolution of the refining gas and subsequent reaction with the impurities inside the melt. Moreover, the effect of the size and velocity of rising gas bubbles on the rate of removal of impurities is not well understood.

In the present investigation an attempt has been made to obtain a clearer picture of the interaction of a bubble with

a liquid metal. Lead has been chosen as the metal because of its relatively low melting point. The effect of bubble size and bubble residence time on the kinetics of dissolution of oxygen in pure lead and subsequently the kinetics of its removal by hydrogen bubbling has been studied. An oxide solid electrolyte concentration cell has been used to measure continuously the concentration of oxygen in the lead during oxidation and reduction.

In Chapter 2, a literature survey of the work done on the interaction between bubbles and liquids, is presented. Chapter 3 deals with the apparatus and experimental procedure. The results are presented and discussed in Chapter 4. Chapter 5 contains the conclusions and finally some suggestions for further work are given in Chapter 6.

CHAPTER 2

LITERATURE SURVEY

2.0 INTRODUCTION

Relatively little work has been done on the study of the interaction between gas bubbles and liquid metals. On the other hand, a large number of papers have been published on the interaction at room temperatures between bubbles and liquids, which are transparent. Since the behaviour of bubbles in liquid metals and in room temperature liquids is essentially the same, a great deal of information can be gained from studies on the interaction at room temperature. Thus a brief comprehensive review of bubble liquid interaction at room temperature is presented prior to the review on the work done on liquid metals. Finally the solid electrolyte e.m.f. method, used to measure concentrations in the present work, is discussed.

2.1 STUDIES ON LOW TEMPERATURE LIQUIDS

Previous studies on low temperature liquids have been concerned with the determination of the following factors in various regimes of bubble motion: a) bubble size and shape, b) bubble velocity and motion, c) mass transfer rates and coefficients across the gas-liquid interface and d) interfacial area for different configurations.

Most of the experimental data and theoretical investigations are mainly concerned with single bubbles rising at

low velocities in the laminar region. Mass transfer between swarms of bubbles in agitated turbulent liquids has not been investigated rigorously.

Size, shape and motion of bubbles. Several workers[1-3] have studied experimentally the shape and motion of air bubbles in water and other liquids. The shape of the bubble and the nature of its motion is determined by the nature of the liquid flow past it. When the bubble size is small (< 2 mm) the Reynolds number is small and the bubble is spherical. With increasing size of the bubble, the Reynolds number also increases and the bubble no longer remains spherical, but assumes an oblate spheroidal shape, the degree of distortion increasing with increasing bubble size. When the bubble size is greater than 7 mm, the motion of the bubble also changes. Whereas bubbles smaller than 7 mm rise in a straight line, those larger than 7 mm either zigzag as they rise or rise in a helical path. Bubbles larger than 8 mm are found to be spherical-cap in shape.

Velocity of bubble. For very small spherical bubbles one may assume a creeping flow around the bubbles as they rise in the liquids. Since there is no slip at the bubble-liquid interface, the normal and tangential stresses and the tangential velocities on both sides of the interface are zero. For these conditions Hadamard[4] and Rybczynski[5] have given a correlation which expresses the drag force F_D as a function of viscosities of the gas and liquid media μ' and μ ,

respectively, the radius of the bubble r_b and the terminal velocity U_∞.

When a spherical bubble is moving at its terminal velocity, the drag force on the bubble must equal the force on it due to buoyancy. This equality has been used to derive the following equation,

$$U_\infty = \frac{2}{9} \frac{g r_b^2}{\mu} (\rho - \rho') \left[\frac{3\mu' + 3\mu}{3\mu' + 2\mu} \right] \qquad (1)$$

where ρ and ρ' are, respectively, the densities of liquid and gas. For gas bubbles rising in liquids $\mu' << \mu$ and $\rho >> \rho'$. Therefore,

$$U_\infty = \frac{1}{3} \frac{g r_b^2}{\mu} \qquad (2)$$

Levich[6] has shown that in the case of very small bubbles, because of the inherent presence of surface active agents in the liquid, internal circulation is stopped because of the agents forming an immobile film on the bubble surface. Hence the bubbles behave as rigid spheres and their rising velocity is given by Stoke's Law.

$$U_\infty = \frac{2}{9} \frac{g r_b^2}{\mu} \qquad (3)$$

With increasing bubble diameter, surface active agents can no longer completely cover the surface and internal circulation occurs. Surface tension forces lose their influence further as the bubble gets distorted at larger sizes. The transition between spherical and ellipsoidal

forms depends on a balance between inertial, viscous and surface tension forces for which no general relationship is yet available.

Calderbank and Lochiel[7] have studied the behaviour of bubbles in a large size range. They have made an attempt to define oblate spheroid bubbles in terms of their shapes. They have expressed the areas of the bubbles as

$$A_{os} = 2\pi a^2 \left[1 + \frac{\ln(E + (E^2-1)^{1/2})}{E\,(E^2-1)^{1/2}} \right] \qquad (4)$$

where a is the semi-major axis of the bubble and E is the eccentricity defined as the ratio of the width of the spheroid to its height. E can be related to a and d_b, the equivalent spherical diameter, since

$$V = \frac{\pi}{6} d_b^3 = \frac{4}{3} \pi \frac{a^3}{E} \qquad (5)$$

Thus by measuring the cross sectional areas of the bubbles by shadow photography, Calderbank and Lochiel could estimate the areas of the ellipsoidal bubbles.

As the size of the bubbles is increased further, they assume spherical cap shapes and for these, mathematical relations have been presented for their terminal velocities.

Davies and Taylor[9] have shown that, for a spherical cap bubble, potential flow can be assumed around the bubble. Accordingly, they derived the following expression for terminal velocity

$$U_\infty = 0.72 \sqrt{g d_b} \qquad (6)$$

where d_b is the diameter of a sphere with volume equal to that of the spherical cap.

Collins[10] showed that the Davies and Taylor[9] analysis for the case of a bubble rising in a thin sheet of liquid leads to the velocity expression,

$$U_\infty = \frac{1}{2}(g\, r_c)^{1/2} \qquad (7)$$

where r_c is the radius of curvature of the spherical surface.

The relations given above are for the terminal velocities of bubbles in a container of infinite width. However, in actual experiments, the container vessels have finite widths and their walls exert a retarding effect on the bubbles. Uno and Kintner[11] studied this problem and found that the actual terminal velocities of the bubbles were given by the expression

$$U = U_\infty \frac{1}{b}\left(1 - \frac{d_b}{d}\right)^{0.765} \qquad (8)$$

where U_∞ is the terminal velocity in a medium of infinite width, d, the diameter of the container vessel and b, a constant which depends on the vessel diameter and surface tension of the liquid.

Mass transfer between the bubble and the surrounding liquid. Hammerton and Garner[12] have shown that the mass transfer coefficients for small spherical bubbles would be those predicted by Frossling[13] for solid spheres

$$K_L = \frac{D}{d_b}(2 + 0.55\, N_{Re}^{0.5} \cdot N_{Sc}^{0.5}) \qquad (9)$$

where D is the diffusion coefficient of the solute in the liquid, N_{Re} is the Reynolds number and N_{Sc} is the Schmidt number. Much higher values are expected when internal circulation begins inside the bubbles and velocity gradients within the liquid at the gas-liquid interface are reduced or eliminated. Hughmark[13] has also postulated a semi-theoretical relation for small bubbles. For a sphere rising through a liquid his theory predicts

$$N_{Sh} = 2 + a_1\left[(N_{Re})^{0.404}\,(N_{Sc})^{0.339}\left(\frac{d_b\, g^{1/3}}{D}\right)^{0.072}\right]^{b_1} \qquad (10)$$

where N_{Sh} is the Sherwood number and a_1 and b_1 are constants. For spherical bubbles $a_1 = 0.061$ and $b_1 = 1.61$.

Higbie[43] has presented a model which predicts the mass transfer coefficient in the following form

$$K_L = 2\left(\frac{D\, U_\infty}{\pi d_b}\right)^{1/2} \qquad (11)$$

For bigger bubbles, the dependence of K_L on the size is not completely understood due to lack of data on distortion, flow pattern etc., and there is no general correlation available for calculating the mass transfer coefficients.

For spherical cap bubbles, Baird and Davidson[15] have shown that K_L for the leading surface is given by

$$K_L = \text{Const.}\; d_b^{-0.25} \cdot D^{0.25} \cdot g^{0.25} \qquad (12)$$

Calderbank[16] has presented the following correlation

$$\frac{2K_L \cdot r_b}{D} = f\left\{\left[\frac{\mu}{\rho D}\right]^{0.5}\left[\frac{2r_b \cdot U_\infty \cdot \rho}{\mu}\right]^{0.766}\right\} \qquad (13)$$

Lochiel and Calderbank[8] have postulated correlations for K_L for spherical as well as spherical cap shapes. Their theory predicts that for a sphere:

$$K_L = 0.8\,(D\,U_\infty / r_b)^{1/2} \qquad (14)$$

where $$U_\infty = 2.9\,(r_b\,g)^{1/3} \qquad (15)$$

and for a spherical cap:

$$K_L = 0.857\,(D\,U_\infty / r_b)^{1/2} \qquad (16)$$

Swarm of bubbles in a liquid. The system of a swarm of bubbles moving in a liquid is a complicated one. The bubbles may be of various sizes and may be dispersed unevenly in the liquid. Moreover, bubble coalescence and break-up may be occurring simultaneously with the rise of bubbles. Thus any attempt at a theoretical correlation for the velocity distribution of the bubbles in a swarm and mass transfer between the liquid and the bubbles must employ many simplifying assumptions. Gal-or and Waslo[17,18] have derived theoretical correlations for very small identical particles which are assumed to be evenly distributed throughout the liquid. The correlations derived by them are, however, of little use for metallurgical systems because the idealised conditions are far from those encountered in real systems.

2.2 STUDIES ON BUBBLE-LIQUID METAL INTERACTION

In metallurgical processes involving gas bubble interaction with liquid metal, three steps are involved in the mass transfer. These are: a) the transport of the species dissolved in the metal to the bubble interface, b) chemical reaction at the interface, and, finally, c) the desorption of the gaseous products and transport of these products from the interface to the bulk of the gas in the bubble. When the mass transfer is from the bubble to the liquid metal, the steps are in the reverse order, namely, a) transport of the gaseous solute in the bubble from the bulk of the gas to the interface with subsequent adsorption at the interface, b) chemical reaction at the interface and, c) transport of the solute from the interface to the bulk of the liquid.

At the high temperatures at which most metals are in the liquid state, the chemical reaction and the desorption or adsorption steps are likely to proceed with rapidity. The rate controlling steps are thus transport of the gaseous species in the bubble or transport of the solute in the liquid metal.

The studies on bubble-metal interaction may be divided into two classes: a) those with small bubbles which are assumed spherical in shape (r_b < 5 mm) and b) those with large spherical-cap bubbles.

Studies with small bubbles. The production of small bubbles in liquid metals and the measurement of concentration changes

in the metals present more difficulties than what are encountered in work at low temperatures. Small bubbles are generally introduced by passing gas through tubes, of materials resistant to wear at high temperatures, immersed in the metals. Thus vycor has been used for liquid aluminium[19], stainless steel for lead[20], and alundum for liquid copper[21].

The bubble after being released in the liquid metal may change dimensions due to the following effects.

1) Thermal expansion if the gas is not at the melt temperature at the time of release.
2) Expansion caused by reduced pressure head as the bubble rises.
3) Expansion due to diffusion of product gas into bubble.
4) Contraction due to diffusion of bubble gas out of bubble.
5) Contraction due to reaction of the metal with bubble gas.

Estimation of bubble size. Pehlke and Bement[19] as well as Bandyopadhyay and Ray[20] estimated the diameter of the bubble just after release, d_b, to be twice the orifice diameter d_o. Experimental work in low temperature liquids shows[22] that at low flow rates this assumption is valid. Manda and Geiger[21], however, used the expression

$$d_b^3 = \frac{6\, d_o \sigma}{g(\rho - \rho')} \qquad (17)$$

where is the surface tension of the liquid. This expression is said to be valid upto N_{Re} of 200 and was applicable in the work of Manda and Geiger who used very low flow rates ranging

from 0.4 to 15 cm^3 sec^{-1} yielding values of N_{Re} between 1 and 90. The expression, of course, states that the bubble size is independent of the flow rate. Bubble diameters obtained from this expression are lesser than twice the orifice diameter. For gas jets Leibson et al[23] have given the following general expression

$$d_b = 0.18 (d_o)^{0.5} (N_{Re_j})^{0.33} \qquad (18)$$

where N_{Re_j} is the jet Reynolds number defined in terms of the dimensions of the orifice. This expression, which applies to N_{Re_j} between 500 to 2000, cannot be used for the data obtained with low flow rates.

Measurement of solute concentration in liquid metal. Several techniques have been used for the measurement of the rate of mass transfer. Pehlke and Bement[19], in their work on the removal of hydrogen from liquid aluminium by flushing argon, used vacuum fusion technique for analysis of the metal samples at different periods. Bandyopadhyay and Ray[20] have used a solid electrolyte cell for a continuous automatic recording of oxygen concentration during oxidation of molten lead by oxygen bubbling. Nanda and Geiger[21] used a similar technique in their studies on oxygen removal from copper by carbon monoxide.

Measurement of mass transfer coefficient. Most of the workers who have studied bubble metal interaction have assumed the rate controlling step to be the transport of the solute in the liquid metal and their results have proved this assumption to be valid

under the experimental conditions used by them.

Bandyopadhyay and Ray[20] worked with only one bubble diameter and obtained a value of 0.035 cm/sec for the mass transfer coefficient of oxygen in lead. Pehlke and Bement[19] using a number of orifice diameters attempted to study the effect of varying bubble size on the mass transfer coefficient. However, they were unable to obtain any coherent relationship. The mass transfer coefficients they obtained varied from 3.5×10^{-2} cm/sec to 6.8×10^{-2} cm/sec. Handa and Geiger[21] also studied the effect of varying bubble diameter and found that the experimentally observed values of the mass transfer coefficient were in good agreement with those obtained from Hughmark's[14] semi-theoretical relationship.

Recently Schenck et al[24] have postulated a mathematical model for the mass transfer of C, O, H, N and S from steel to bubble of argon assuming that all these impurities are removed from the steel in gaseous form. They considered the simultaneous mass transfer of the elements as a function of the initial bubble mass, height of the steel bath, the bulk concentrations in the melt, and the external pressure. To compute the amount of mass transfer of the various elements they calculated the bubble velocities and liquid phase mass transfer coefficients for both spherical and spherical-cap bubbles from equations postulated by workers essentially for low temperature liquids.

However, despite the work done by the above workers, the interaction of bubbles with liquid metals, when the size of the

bubble is small so that it can be considered spherical, has not yet been fully understood. The effect of certain variables such as bubble size, flow rate of gas and temperature has not been studied rigorously. An attempt will be made in this work to gain a fuller understanding of the interaction and if possible to find a correlation which expresses mass transfer coefficient in terms of the various experimental variables.

Studies on large spherical-cap bubbles. Large bubbles encountered in metallurgical processes may often be considered to have spherical-cap shape. In recent years, several workers[25-27] have studied the behaviour and interaction of spherical-cap bubbles in liquid metals. All have used similar techniques for bubble generation and bubble velocity measurement. Single bubbles are formed by injecting gas into a hemispherical inverted cup which is then rotated mechanically to release the bubble.

There is no definite way of estimating the bubble size and shape for the spherical-cap bubbles. Davenport, Bradshaw and Richardson[25] used electrical probes to measure the bubble size in mercury, but could not repeat the technique with high temperature liquid metals.

Measurement of rising velocity. The bubble velocity is usually measured by measuring the pressure variations in the 'top space' (the space between the liquid metal surface and roof of the container vessel) as the bubble rises through the metal. A definite 'kink' in the plot of pressure vs. time occurs when the bubble surfaces and, knowing the height of the rise of the

bubble, its velocity can then be calculated[25,27].

Measure of mass transfer coefficient. All the workers studying the interaction of spherical-cap bubbles with liquid metals have used the system oxygen-silver. The rate of absorption of oxygen is given by[27]

$$\frac{dn_G}{dt} = K_L \, a_b \, (C_s - C) \qquad (19)$$

where C and C_s refer to the concentrations of oxygen in the bulk and at the interface, respectively. The above equation may be rewritten in terms of pressure and volume changes in the bubble to give[27]

$$P \frac{dV}{dt} + V \frac{dP}{dt} = K_L \, S V^{2/3} \, RT \, (C_s - C) \qquad (20)$$

where S is a shape factor expressed as

$$S = a_b / V^{2/3} = (36\pi)^{1/3} \qquad (21)$$

From Sievert's law,

$$C_s = q \sqrt{P} \qquad (22)$$

where q is Sievert's law constant. The bubble volume has been expressed as

$$V = v (1 - p_1/p) \qquad (23)$$

where v is the volume of the 'top space', p_1 the pressure in 'top space' before the introduction of gas in the cup and p is the pressure of the 'top space' in general. Differentiating,

$$\frac{dV}{dt} = \frac{vp_i}{p^2} \cdot \frac{dp}{dt} \qquad (24)$$

The pressure in the bubble is given by

$$P = p + b_2 h \qquad (25)$$

where b_2 is a constant and h is the melt height.

Since $\frac{dh}{dt} = -U_\infty$, $\frac{dP}{dt} = \frac{dp}{dt} - b_2 U_\infty$ (26)

Thus the following equation is arrived at

$$\left(1 + \frac{p_i}{p^2}\right) b_2 h\, v^{1/3} \frac{dp}{dt} - v^{1/3} \left(1 - \frac{p_i}{p}\right) b_2$$

$$= K_L\, SRT \left(1 - \frac{p_i}{p}\right)^{2/3} \left[q(p + b_2 h) - C \right] \qquad (27)$$

Consequently, the mass transfer coefficient is calculated in terms of p, $\frac{dp}{dt}$, the rising velocity U_∞ and the time after release of the bubble. The rising velocity has been calculated by all workers using Davies and Taylor[9] correlation

$$U_\infty = 1.02 (gr_c)^{1/2} \qquad (28)$$

where r_c is the radius of curvature of the leading surface. At small values of r_c, the observed velocities were found to agree reasonably well with the theoretical velocities predicted by Eq. (28) but at larger values the workers found that the wall effects retarded the motion of the bubbles and the velocities fell below the theoretical values. However, when the wall effects were accounted for, using Uno and Kintner's[11] correlation the discrepancy between observed and theoretical velocities was found

to be negligible. Davenport, Bradshaw and Richardson[25] and Paneni and Davenport[26] have observed that the velocities of bubbles in liquid metals as well as in aqueous liquids are compatible. They have concluded that neither the surface tension nor the density of the liquid has any noticeable effect on the rising velocity.

Mass transfer coefficient and bubble size. Davenport, Bradshaw and Richardson[25] have calculated K_L for silver-oxygen system for different values of bubble size and compared the measured variation with the theoretical variation predicted by the Baird and Davidson[15] equation

$$K_L = \text{Const.}\ d_b^{-0.25} \cdot D^{0.25} \cdot g^{0.25} \qquad (29)$$

They obtained slightly higher values for K_L because of the total oxygen transfer. The theory allows transfer only across the front spherical surface. In addition, it has been observed that the trailing edge of the spherical-cap bubble is rippled and the rippling apparently enhances mass transfer.

2.3 USE OF A SOLID ELECTROLYTE CELL FOR KINETIC MEASUREMENTS

In an oxygen-liquid metal system the oxide solid electrolyte cell provides a quick and reliable means for a continuous measurement of the oxygen concentration.

In recent years, solid electrolyte cells have begun to find a wide application for the studies of the kinetics of various reactions, such as defect structure of ferrites[28], diffusion in metals[29-34], condensation and evaporation reactions

in certain sulphides and selenides[35,36] and rate constants of gas-solid reactions[30,37-39].

In the present investigation, the solid electrolyte used is stabilised zirconia (10 mole per cent CaO) which has been proved to exhibit complete ionic conductivity ($t_{ion} > 0.99$) over a wide range of oxygen pressure (0 to 10^{-15} atm[44]). Recently, Goto et al[40] working with a zirconia solid electrolyte cell of the type:

$$\text{Air} \;\vdots\; \text{Liquid Ag} - \underline{O} \mid ZrO_2 \cdot CaO \mid \text{Liquid Ag} - \underline{O} \;\vdots\; \text{Air}$$

compared the rate of the metal-electrolyte interface reaction, $O^{2-} = \underline{O} + 2e$, with the rate of oxygen transfer in liquid silver, and found the former to be much faster. Thus in the present work, equilibrium will always be attained between the adsorbed oxygen at the liquid lead-electrolyte interface and the oxygen dissolved in the liquid lead, and the e.m.f. of the cell

$$Ni \mid NiO \mid ZrO_2 \cdot CaO \mid Pb(O)$$

will give the average oxygen concentration of the melt.

Estimation of the oxygen content from the e.m.f. values in molten lead has been done by Alcock et al[41] through a study of a similar type of cell. They found that the saturation concentration of oxygen in lead was

$$\log_{10} (\text{N Pb} \cdot \text{at.}\,\% \; O) = -\frac{5240}{T} + 4.55 \qquad (30)$$

They also observed that oxygen obeyed Henry's law in dilute solution of oxygen in lead upto its solubility limit. This establishes the basis for calculation of oxygen concentration in lead from the e.m.f. data.

CHAPTER 3

APPARATUS AND EXPERIMENTAL PROCEDURE

The apparatus used in the present work was fabricated by Bandyopadhyay and is explained in detail in his thesis[20]. It consisted of

a. The furnace consisting of the reaction tube and the power supply arrangement
b. The gas purification train
c. The arrangement for control of gas composition and measurement of gas flow rates
d. Appliances for measuring and recording the e.m.f.

3.1 THE FURNACE AND THE POWER SUPPLY ARRANGEMENT

The furnace consisted of six 22" long vertical globar heating elements in a cylindrical shell which was packed with a mixture of asbestos powder and small pieces of firebrick to provide the insulation. The globars had each a 10" long hot zone and a resistance of 0.83 ohms. The furnace was designed to operate upto a maximum of 1200°C with a surface temperature of 150°C.

The power supply and temperature controller assembly consisted of a Leeds-Northrup Electromax 4320 temperature controller, two Dimmerstat variacs of a maximum current capacity of 15 amps each, one A-B type Leeds-Northrup contactor and a number of Bajaj voltmeters and ammeters (Figure 1).

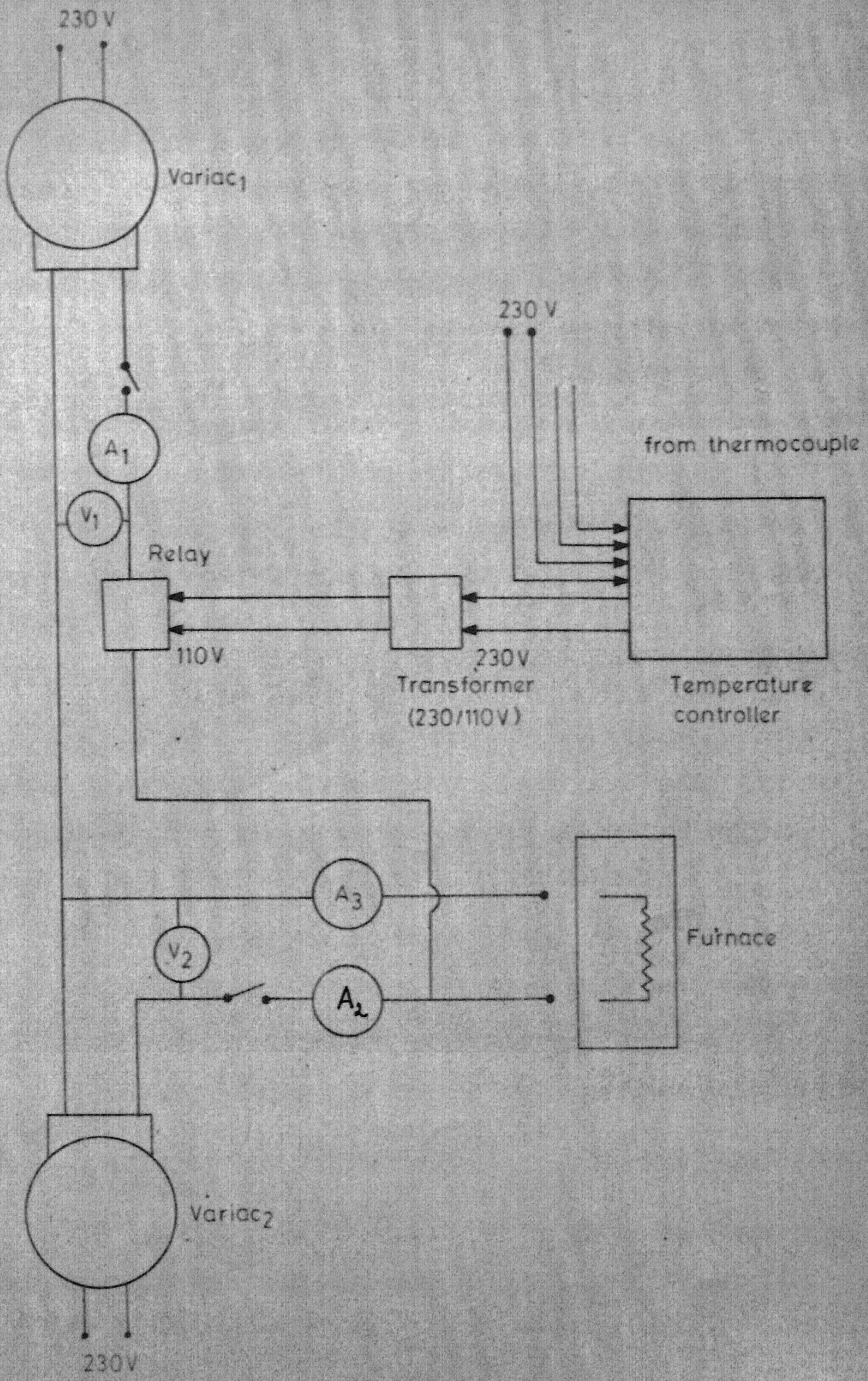


FIG. 1 SCHEMATIC DIAGRAM OF THE POWER SUPPLY UNIT

Because of a considerable decrease in resistance of the globars at higher temperatures, the current drawn by them exceeded 15 amps. The two variacs were thus connected in parallel and shared the load when the temperature was below the set point. However, when the temperature exceeded the set point the temperature controller went off thus opening the contactor and causing only one variac to take the whole load and only a fraction of the initial power was dissipated in the heating elements.

The furnace tube was made of inconel 2½" I.D. and 3" O.D. For cooling the inconel tube, coils of copper tubing were soldered at the top and bottom.

3.2 THE GAS PURIFICATION TRAIN

It was necessary to maintain a neutral atmosphere over the reference electrode in the solid electrolyte cell. The gas purification train was fabricated for the purpose of removing traces of oxygen and water-vapour from the argon gas.

The inert argon gas was successively passed through a series of $CaCl_2$ drying towers, a copper gauge furnace maintained at 600°C and finally through a titanium chip furnace at 800°C.

A schematic diagram of the gas train is given in Figure 2.

3.3 ARRANGEMENT FOR CONTROL OF GAS COMPOSITION AND MEASUREMENT OF GAS FLOW RATES

The gas flow rates were measured by capillary flowmeters which were in turn calibrated against a wet-test meter. Two capillary flowmeters were used, one to register the flow rate of

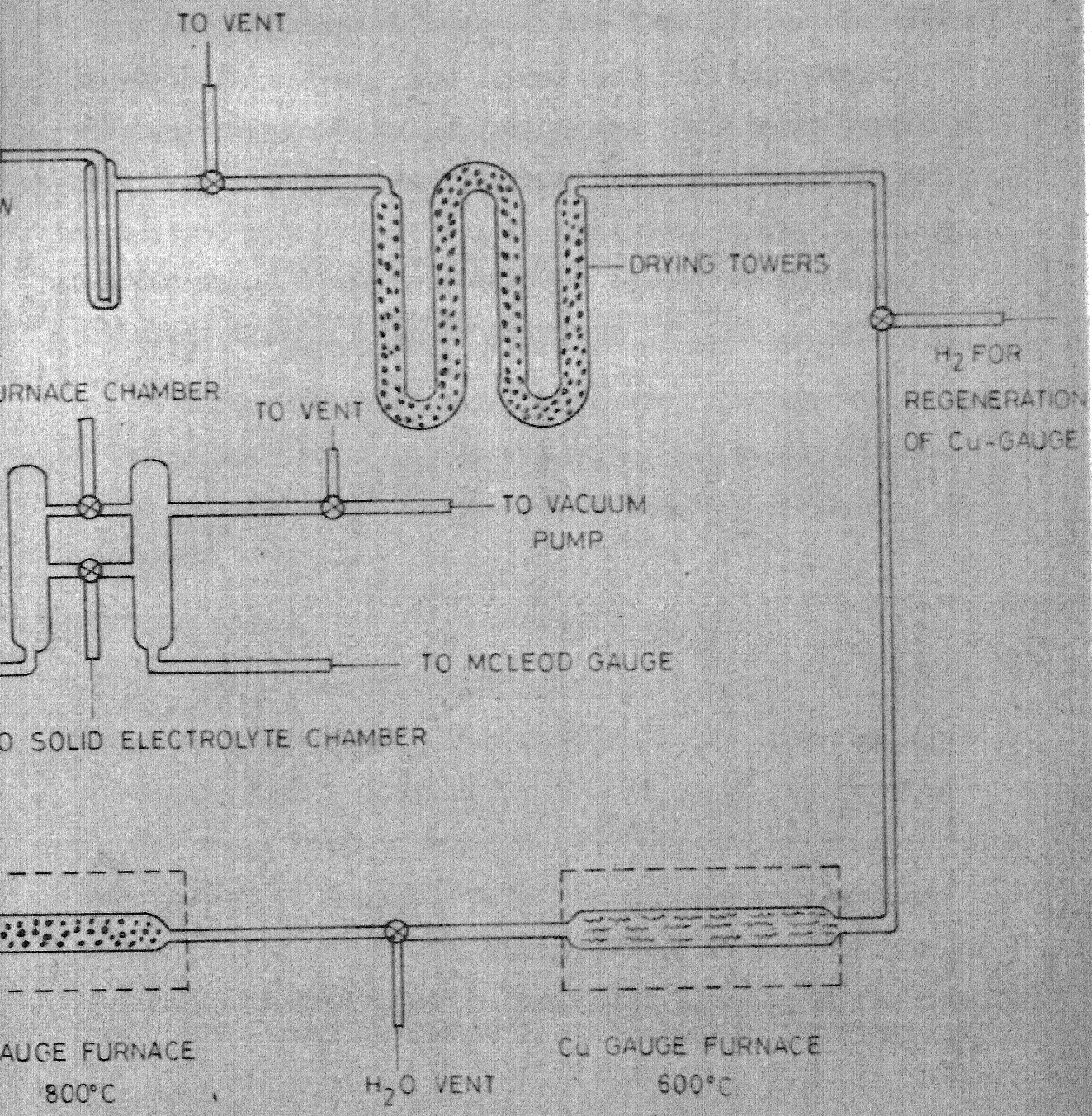


FIG. 2 GAS PURIFYING TRAIN

argon and the other to register the flow rate of the mixture of argon and oxygen. The oxygen flow rate was measured by counting the number of bubbles flowing in a given period of time through a bubbler. The two gases, oxygen and argon, were mixed in a nozzle type oxy-acetylene torch. Tests by Bandyopadhyay[20] confirmed that the mixing was complete. A schematic diagram of the arrangement is given in Figure 3.

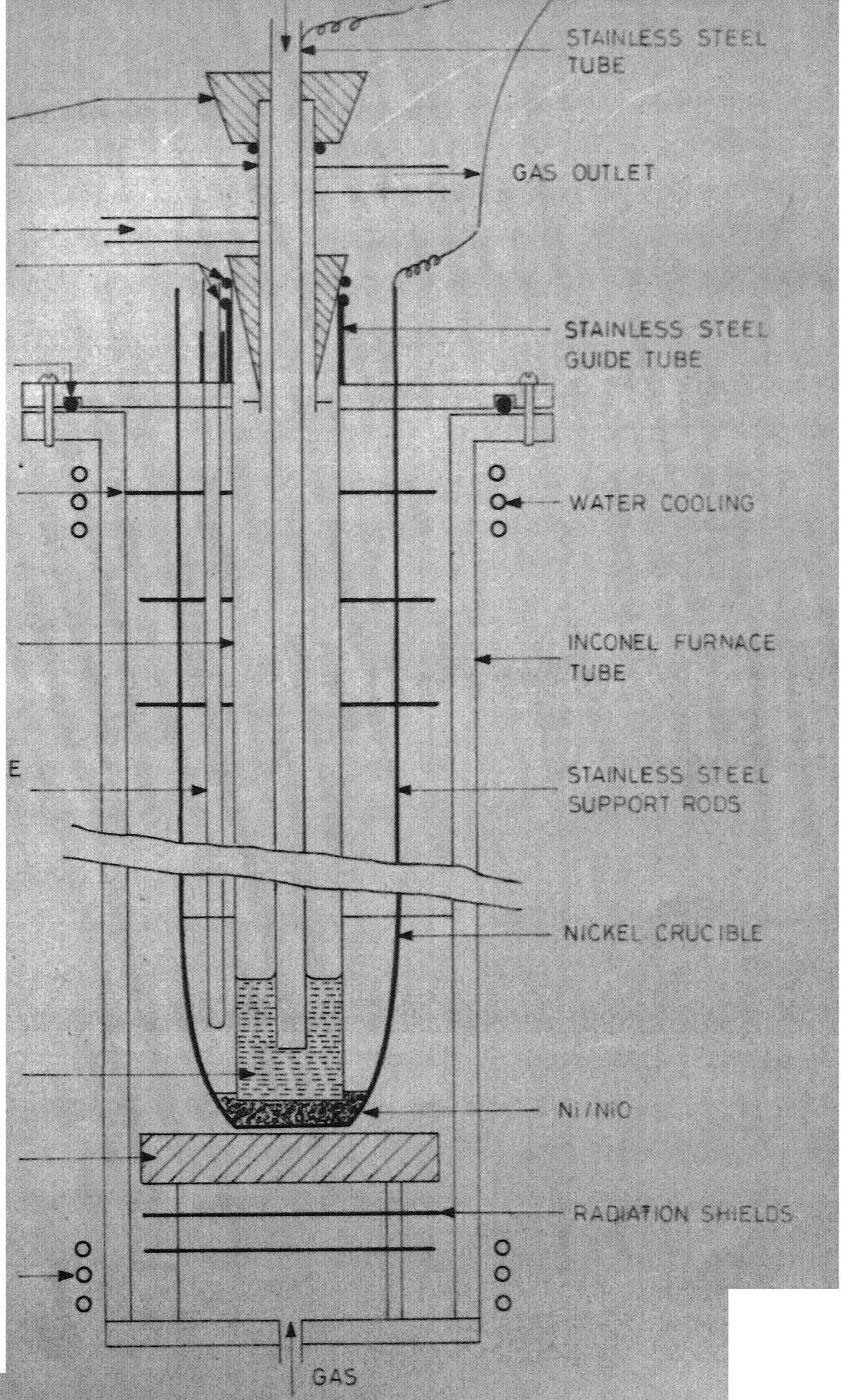
During reduction runs, the argon inlet was closed and hydrogen was passed through the oxygen inlet, its flow rate being measured by flowmeter-2 which was also calibrated for hydrogen.

3.4 THE EMF MEASURING AND RECORDING DEVICES

During both oxidation and reduction runs, the e.m.f. changed continuously and was recorded on the chart paper of a Sargent recorder model SRL having an input impedance of 50 Kilo ohms. This high input impedance ensures that no polarisation of the cell occurs during measurement. The sensitivity of the self balancing bridge of the recorder is very high and thus there is negligible time lag in the recorded voltage.

3.5 THE CELL ASSEMBLY

The cell (Figure 4) consisted of a 24" long calcia-stabilised zirconia tube, supplied by the Zirconium Corporation of America, Solon, Ohio. The tube was closed at one end (flat)


STAINLESS STEEL TUBE
GAS OUTLET
STAINLESS STEEL GUIDE TUBE
WATER COOLING
INCONEL FURNACE TUBE
STAINLESS STEEL SUPPORT RODS
NICKEL CRUCIBLE
Ni/NiO
RADIATION SHIELDS
GAS

and had an I.D. of 1.5 cm and a wall thickness of about 1.5 mm. It was made from zircoa-B grade material which has a composition of 10 mole per cent CaO and the rest zirconia with traces of other oxides. This material is described as fully stabilised in the cubic crystal configuration and able to retain its crystal structure even on repeated cycling.

On either side of the solid electrolyte tube were electrodes, each completely isolated from the other. The outside electrode consisted of a Ni/NiO mixture kept in a nickel crucible which was spot welded to three stainless steel rods. The rods served the dual purpose of holding the whole assembly in the hot zone of the furnace as well as acting as leads for the Ni/NiO electrode.

The electrode inside the solid electrolyte tube consisted of lead with its dissolved oxygen. A stainless steel tube dipped into the molten lead and served as the outlet of the gas bubbles as well as the lead for the inner electrode.

3.6 EXPERIMENTAL PROCEDURE

Nickel powder (99.99 per cent pure) supplied by Semielements Inc., U.S.A. and black nickel oxide powder (A-R grade) supplied by Cometo Chemicals (Bombay) were mixed in an agate mortar to a 50:50 proportion by volume. This mixture was put in the nickel crucible and pieces of lead sheet were added on top. This lead melts at high temperature and acts as a protective cover for the Ni/NiO mixture, preventing reduction of NiO.

Inside the solid electrolyte tube, was put pure lead (99.99 % pure) and the cell assembly was placed in the furnace. All points where the rubber tubing was connected to the metal tubes, were sealed with black sealant (Cement Picein supplied by Sargent Co., U.S.A.). The black sealant was vacuum tight at the experimental temperatures. When the sealant hardened, the two electrode chambers were evacuated at room temperature and slowly flushed with purified argon. The furnace was then heated and on reaching a temperature of about 150°C, the two chambers were again evacuated to remove any moisture. Pure argon was again flushed and the cell heated to the desired temperature in about 10-12 hours.

The reversibility of the cell used in the present work has been established by Bandyopadhyay[20]. In this work, kinetic studies were performed using three orifice diameters of 0.48 cm (3/16"), 0.32 cm (1/8") and 0.16 cm (1/16"). When the desired temperature was reached, the molten lead was usually found to be unsaturated with oxygen. The oxygen was further reduced by bubbling hydrogen through the melt until a very low e.m.f. ($\sim$ -240 mV) was reached. The hydrogen was then turned off and the melt flushed with purified argon for one hour to drive off any hydrogen remaining in the chamber or the connecting tubes. Thereafter a purified stream of argon was allowed to enter the side inlet tube and the molten lead allowed to equilibrate for $\sim$ 4 hours. When a steady e.m.f. was attained, the argon was shut off and the inner chamber was closed. Argon and oxygen flows were put on and their flow rates adjusted to the desired

values, the gases at this time being allowed to pass through an outlet vent into the air. When the gas mixture composition was accurately controlled the inner chamber was opened to the argon-oxygen mixture. The recorder was immediately turned on with the highest chart speed and the changing e.m.f. was recorded as a function of time. When the cell e.m.f. approached the equilibrium value the argon-oxygen flow was stopped and the melt was flushed with argon to prevent any over-oxidation.

The melt was again kept under purified argon for ~ 2 hours and then the chamber was closed. Hydrogen flow was adjusted to the desired value and the chamber opened to hydrogen, the changing e.m.f. again being recorded until a low constant value was reached. The melt was again flushed with pure argon and the whole procedure repeated for another oxidation and then reduction run.

During all this time, the reference electrode was kept under a steady flow of purified argon.

It was found that despite the protective covering of lead, the Ni/NiO mixture got reduced after about 10 days. The cell was then cooled to room temperature and the Ni/NiO mixture was replaced by a fresh one after which the same procedure was followed as described before.

CHAPTER 4

RESULTS AND DISCUSSION

4.1 THEORETICAL BACKGROUND

Prior to the presentation of the results, the mathematical formulation of the bubble-metal interaction done by Pehlke and Bement[19] will be presented and discussed for the present system.

As has been mentioned earlier, the bubble-metal interaction involves the following steps:

1. transport of oxygen (or water vapour in the case of reduction) in the bubble,
2. adsorption (or desorption) of atomic oxygen at the bubble-metal interface,
3. reaction at the interface, and
4. transport of the dissolved oxygen from the interface to the bulk of the liquid metal (or from the bulk to the interface).

At the high temperatures used in the present work, steps (2) and (3) are likely to be too fast to be rate controlling. Themelis and Schmidt[42], while studying the removal of oxygen from molten copper by single bubbles of carbon monoxide found step (1) to be rate controlling. Bandyopadhyay and Ray[20], however, while studying the oxidation of liquid lead, found mass transfer rates to be independent of the partial pressure of oxygen within a range of 0.03 to 0.17 atmospheres. Thus in the present system, in which the oxygen partial pressures used

are in the same range as those used by Bandyopadhyay and Ray,[20] the step most likely to be rate controlling is the transport of the solute in the liquid metal. The rate of dissolution of oxygen from a bubble of the argon-oxygen mixture into the molten lead is then given by

$$\frac{dn_g}{dt} = K_L \, a_b \, (C_s - C) \qquad (1)$$

where n_g = number of moles of oxygen being dissolved.

K_L = mass transfer coefficient

a_b = area of the bubble metal interface

C_s , C = concentration of oxygen in the lead at the interface and in the bulk, respectively.

For the removal of oxygen from the lead by hydrogen, the equation will be

$$\frac{dn_g}{dt} = K_L \, a_b \, (C - C_s) \qquad (2)$$

Handa and Geiger[21] in their study on the removal of oxygen from molten copper by carbon monoxide observed that in each bubble, nowhere near the equilibrium amount of carbon dioxide, with respect to the bulk oxygen content was produced. This will obviously be the case in any bubble-metal system where the residence time of the bubble in the melt is very small. Thus in the present system, during hydrogen reduction of the liquid lead, the concentration of oxygen in the melt at the bubble-liquid interface may be considered to be that in equilibrium with a gas containing only a small fraction of H_2O. Under these circumstances the concentration of oxygen

at the interface C_s may be assumed to be essentially zero. Equation (2) then reduces to

$$\frac{dn_g}{dt} = K_L \, a_b \, C \qquad (3)$$

Since the treatment is essentially the same for both oxygen dissolution and oxygen removal, henceforth only oxygen dissolution will be considered. In the system studied in the present work, mass transfer can also occur across the free surface of the lead melt. This is given by

$$\frac{dn_g}{dt} = D \cdot A_s \cdot \frac{dC_L}{dx} \qquad (4)$$

where D = diffusion coefficient of oxygen in liquid lead

A_s = surface area of the melt

or $$\frac{dn_g}{dt} = \frac{D}{\delta} A_s (C_s - C) \qquad (5)$$

where δ = boundary layer thickness.

The total rate of transfer is then given by

$$\left(\frac{dn_g}{dt} \right)_{total} = n K_L a_b \, C + A_s \frac{D}{\delta} \Delta C \qquad (6)$$

where ΔC denotes $(C_s - C)$ and n, the number of bubbles in the melt at any time. n is given by

$$n = \frac{F \tau_r}{V} \qquad (7)$$

where F = flow rate of gas

τ_r = time of residence of the bubble inside the melt

and V = volume of the bubble.

It will be appropriate at this time to list the assumptions made on the bubble size and shape. It has been assumed that the bubble that detaches from the orifice is spherical, its diameter just before it detaches from the orifice is twice the orifice diameter and there is no change in the diameter of this bubble as it rises through the melt. The last assumption is reasonably valid if the melt height is small so that the change in the pressure head and the diffusion of gas out of (or into) the bubble is negligible. The size of the bubble just before it detaches from the orifice has been assumed by both Pehlke and Bement[19] and Bandyopadhyay and Ray[20] as twice the orifice diameter. Experimental work in low temperature aqueous liquids by Jackson[22] has also shown this assumption to be valid. In the present work also, bubbles of argon were observed in water contained in vessel with the same geometry as that used in the actual work. It was seen that the bubble size was approximately twice the orifice diameter. However, it was observed that although the shape of the bubble was spherical for the smallest orifice diameter, the bubble that detached from the 1/8" diameter orifice was oblate spheroidal, while the bubble which detached from the 3/16" diameter orifice was spherical-cap. Although it is difficult to say as to how closely the room temperature experiments represent the actual state of the bubble in the lead melt, it seems reasonable to assume that the largest bubble was a spherical-cap and not a sphere.

The surface area of a spherical bubble is

$$a_b = 4\pi r_b^2 \tag{8}$$

while that of a spherical-cap bubble is given by[9,15]

$$a_{curved\ surface} = 11.675\ r_b^2 \tag{9}$$

$$a_{flat\ surface} = 9.508\ r_b^2 \tag{10}$$

where r_b is the radius of a sphere having a volume equivalent to that of the spherical-cap bubble. The calculation of the surface area of an oblate spheroidal bubble requires the measurement of its eccentricity and in the present work this was not possible. The oblate spheroidal bubbles were assumed spherical in shape and their surface area was calculated accordingly. It will be shown later that the error in using this assumption is very small.

The total instantaneous area, na_b, for spherical bubbles is given as

$$na_b = A_b = 3F\tau_r/r_b \tag{11}$$

For a spherical-cap bubble the total instantaneous area is

$$na_{s-c} = A_{s-c} = \frac{F\tau_r}{V}(11.675\ r_b^2 + 9.508\ r_b^2) \tag{12}$$

and since the volume of the bubble is assumed the same as the volume when the bubble is about to detach from the orifice,

$$V = \tfrac{4}{3}\pi r_b^3 \tag{13}$$

in which case

$$A_{s-c} = \frac{F}{\frac{4}{3}\pi r_b} (11.675 + 9.508) \qquad (14)$$

Combining equations (6), (11) and the following equations

$$n_g = V_m (C - C_o) \qquad (15)$$

$$\frac{dn_g}{dt} = V_m \left(\frac{dC}{dt} \right) = - V_m \frac{d \Delta C}{dt} \qquad (16)$$

where V_m is the volume of the melt and C_o the initial concentration of oxygen in its bulk, the following equation is arrived at for spherical bubbles

$$\frac{d \Delta C}{\Delta C} = - \frac{1}{V_m} \left(\frac{D}{\delta} A_s + \frac{3 K_L \cdot F \cdot \gamma_F}{r_b} \right) dt \qquad (17)$$

which on integration yields

$$\ln \left[\frac{C_s - C}{C_s - C_o} \right] = - \frac{1}{V_m} \left[\frac{D}{\delta} A_s + \frac{3 K_L . F . \gamma_F}{r_b} \right] t \qquad (18)$$

In the case of a spherical-cap bubble, the mass transfer occurs across the leading spherical surface as well as across the trailing flat surface. The mass transfer across the flat surface is estimated[27,45,46], such that

$$K_{L,flat} = 0.1 K_{L,curved} \qquad (19)$$

Thus for spherical-cap bubbles equation (6) becomes

$$\left(\frac{dn_K}{dt} \right)_{total} = n K_{L,curved} a_{curved} C + n K_{L,flat} a_{flat} \Delta C + A_s \frac{D}{\delta} \Delta C \qquad (20)$$

which when combined with equations (9), (10), (15) and (16) gives

$$\frac{d\,\Delta C}{\Delta C} = -\frac{1}{V_m}\left[\frac{D}{\delta}A_s + \frac{3.016\,K_L\,F\,\tau_r}{r_b}\right]dt \qquad (21)$$

Integrating,

$$\ln\left[\frac{C_s - C}{C_s - C_o}\right] = -\frac{1}{V_m}\left[\frac{D}{\delta}A_s + \frac{3.016\,K_L\,F\,\tau_r}{r_b}\right]t \qquad (22)$$

A comparison between equations (18) and (22) which are for spherical and spherical-cap bubbles respectively, shows that the only difference between them is in the constants which are 3 and 3.016 respectively. Thus, for oblate spheroidal bubbles, which have a surface area intermediate between the area of a spherical bubble and that of a spherical-cap, the error involved in assuming the oblate spheroids as spheres will be small.

Equations (18) and (22) are for the case when the oxygen is being dissolved into the lead melt. In the case of oxygen removal by hydrogen reduction the equations become

$$\ln\left[\frac{C - C_s}{C_o - C_s}\right] = -\frac{1}{V_m}\left[\frac{D}{\delta}A_s + \frac{3K_L\,F\,\tau_r}{r_b}\right]t \qquad (23)$$

for a sphere, and as mentioned before, since C_s is assumed to be zero

$$\ln\left(\frac{C}{C_o}\right) = -\frac{1}{V_m}\left[\frac{D}{\delta}A_s + \frac{3K_L\,F\,\tau_r}{r_b}\right]t \qquad (24)$$

For a spherical-cap,

$$\ln\left(\frac{C}{C_o}\right) = -\frac{1}{V_m}\left[\frac{D}{\delta}A_s + \frac{3.016\,K_L\,F\,\tau_r}{r_b}\right]t \qquad (25)$$

Thus, if transport of solute in the liquid metal is actually the rate controlling step, then plots of log (C_s-C) against time for oxidation and of log (C) against time for reduction should be straight lines. This has been found to be the case in the present work.

The estimation of the mass transfer coefficient K_L from the slopes of the plots of log (C_s-C) against time and log (C) against time requires a knowledge of the time of residence τ_r of the bubbles in the melt. τ_r is calculated by dividing the height of rise of the bubble by its rising velocity

$$\tau_r = \frac{h}{U} \qquad (26)$$

where U has been estimated using the following equation

$$U_\infty = \left[\frac{\frac{4}{3} g (\rho - \rho') d_b}{0.44 \rho} \right]^{1/2} \qquad (27)$$

for spherical bubbles[47], and

$$U_\infty = 0.72 (g d_b)^{1/2} \qquad (28)$$

for spherical-cap bubbles[9], making the necessary correction for wall effects using the equation

$$\frac{U}{U_\infty} = \left[\frac{1}{b} \left(1 - \frac{d_b}{d}\right) \right]^{0.765} \qquad (29)$$

4.2 RESULTS AND DISCUSSION

Hydrogen Reduction Runs The changing e.m.f. observed during the hydrogen reduction runs was converted to oxygen concentrations

and these are given in Tables 2-5. From the concentrations, values of log (C) have been calculated and plotted against time. These plots are shown in Figures 5-8.

It is seen that the rate of change of concentration increases initially, attains a constant value and then, at very low concentrations of oxygen, decreases to nearly zero. In the intermediate region equations (24) and (25) hold good and the mass transport of oxygen in liquid lead is the rate determining step. In the initial stages, the change in the rate of oxygen removal might be due to the fact that it takes time for the hydrogen gas to completely displace the inert argon gas from the inner chamber of the solid-electrolyte cell. Initially the bubble coming in contact with the liquid lead is almost pure argon. Gradually, the hydrogen content of the bubble increases and as more hydrogen comes in contact with the liquid lead, the amount of oxygen removed also increases, till finally the bubble consists solely of hydrogen and a steady rate of removal of oxygen is attained. The decrease in the rate of oxygen removal at the end of each run may be due to the fact that as the concentration of oxygen in the molten lead decreases the bulk concentration approaches the concentration at the interface which is actually not zero as has been assumed but has some finite value. Initially the bulk concentration of oxygen is much greater than the concentration at the interface and although the difference between the two is decreasing as the run proceeds it is large enough to maintain the driving force for oxygen transport to the bubble-metal interface. However, when the bulk

TABLE 2

HYDROGEN REDUCTION OF OXYGEN SATURATED LEAD

Temperature : 700°C Orifice dia. : 0.16 cm

Flow rate (cc/min)

175.8			123.4			74.8		
Time (secs)	EMF (mV)	Concentration (atom /)	Time (secs)	EMF (mV)	Concentration (atom /)	Time (secs)	EMF (mV)	Concentration (atom /)
0	137.4	0.097502	0	147.1	0.123006	0	133.6	0.089132
30	131.2	0.085314	30	142.9	0.111203	60	128.4	0.079621
60	124.8	0.072443	60	139.2	0.101901	90	125.2	0.073114
90	117.9	0.061381	90	134.2	0.091830	120	122.0	0.067612
120	110.3	0.051174	120	130.5	0.082992	150	119.0	0.062950
150	101.4	0.041502	150	126.7	0.075684	180	115.1	0.057413
180	88.3	0.030341	180	123.0	0.069021	210	111.5	0.052722
195	80.4	0.025123	210	118.7	0.062521	240	107.4	0.047750
210	68.9	0.019104	240	113.9	0.055723	270	102.9	0.042951
225	56.2	0.014090	252	111.5	0.052722	300	98.1	0.038281
231	50.7	0.012362	264	109.6	0.050351	330	92.8	0.033733
237	41.7	0.009977	276	106.3	0.046562	360	86.8	0.029242
246	28.3	0.007244	288	101.9	0.041883	390	79.7	0.024663
249	16.7	0.005495	300	97.8	0.038020	420	68.8	0.019051
252	8.9	0.004571	312	92.5	0.033342	450	55.1	0.013714
255	-6.5	0.003162	324	88.8	0.030690	462	45.6	0.010962
258	-18.2	0.002399	336	82.5	0.026301	474	36.9	0.008913
261	-31.7	0.001738	348	70.9	0.020043	480	30.0	0.007551
264	-45.1	0.001262	360	57.3	0.014452	486	18.6	0.005754
267	-49.1	0.001148	366	41.7	0.009977	492	7.0	0.004365
270	-54.9	0.001000	372	25.5	0.006761	498	1.1	0.003802
273	-60.5	0.000875	378	12.0	0.004920	504	-2.7	0.003467
276	-66.1	0.000764	384	-6.5	0.003162	510	-8.5	0.003020
279	-76.0	0.000605	390	-8.3	0.003013	516	-18.2	0.002399
282	-81.9	0.000525	396	-14.1	0.002636	522	-25.9	0.001995

(contd.)

Flow rate (cc/min)

175.8		123.4			74.8		
EMF (mV)	Concentration (atom /)	Time (secs)	EMF (mV)	Concentration (atom /)	Time (secs)	EMF (mV)	Concentration (atom /)
- 97.3	0.000363	402	- 30.6	0.001782	528	- 35.6	0.001585
-109.8	0.000274	408	- 43.0	0.001324	534	- 47.2	0.001202
-118.1	0.000222	414	- 54.6	0.001007	540	- 62.6	0.000832
-126.3	0.000182	420	- 75.2	0.000617	546	- 64.5	0.000794
-137.4	0.000140	426	- 90.1	0.000431	552	- 68.9	0.000718
-153.4	0.000096	432	-108.7	0.000276	558	- 78.0	0.000578
-171.0	0.000063	438	-120.7	0.000209	564	- 89.7	0.000439
-195.9	0.000035	444	-132.1	0.000159	570	- 99.2	0.000347
-216.0	0.000021	450	-143.2	0.000122	576	-107.4	0.000286
-222.6	0.000018	456	-157.3	0.000087	582	-114.8	0.000240
-224.8	0.000017	462	-173.0	0.000060	588	-124.4	0.000191
-227.9	0.000016	468	-182.7	0.000048	594	-130.2	0.000166
-230.6	0.000015	474	-194.4	0.000036	600	-138.2	0.000134
-233.8	0.000014	480	-203.7	0.000029	606	-147.6	0.000110
-240.2	0.000012	486	-211.5	0.000024	612	-161.0	0.000079
-244.6	0.000011	492	-218.1	0.000020	618	-168.9	0.000066
-246.1	0.000011	504	-221.1	0.000019	624	-174.7	0.000058
-246.9	0.000010	516	-223.1	0.000018	630	-178.7	0.000052
		528	-227.3	0.000016	636	-184.4	0.000046
		540	-230.6	0.000015	642	-190.3	0.000040
		570	-236.3	0.000013	648	-195.7	0.000035
		600	-239.1	0.000012	654	-197.1	0.000034
		630	-243.2	0.000011	660	-198.6	0.000033
		660	-245.4	0.000011	672	-203.7	0.000029
					684	-209.6	0.000025
					696	-213.5	0.000023
					708	-217.2	0.000021
					720	-219.3	0.000020
					750	-228.8	0.000016
					780	-233.8	0.000014
					810	-238.1	0.000013
					840	-241.2	0.000012
					900	-245.9	0.000010

TABLE 3

HYDROGEN REDUCTION OF OXYGEN SATURATED LEAD

Temperature : 700°C Orifice dia. : 0.32 cm

Flow rate (cc/min)

104.9		183.0			86.5		
EMF (mV)	Concentration (atom /)	Time (secs)	EMF (mV)	Concentration (atom /)	Time (secs)	EMF (mV)	Concentration (atom /)
36.9	0.008913	0	153.9	0.144505	0	149.0	0.128813
28.3	0.007244	120	143.2	0.112203	120	140.8	0.105921
1.5	0.003828	240	133.6	0.089133	240	132.6	0.087102
-4.3	0.003412	360	121.4	0.066834	360	122.3	0.067614
-19.1	0.002344	420	110.4	0.051293	480	109.3	0.050120
-34.6	0.001622	480	69.5	0.019950	600	93.0	0.033882
-54.1	0.001023	504	37.9	0.009120	720	69.5	0.019951
-70.4	0.000692	528	8.9	0.004571	780	55.8	0.013802
-87.5	0.000459	564	-33.2	0.001675	840	31.4	0.007762
-107.0	0.000288	576	-49.1	0.001148	864	18.6	0.005754
-126.3	0.000182	588	-72.5	0.000656	888	-1.5	0.003565
-143.9	0.000120	600	-91.0	0.000423	912	-20.1	0.002291
-162.9	0.000076	612	-110.1	0.000269	936	-40.4	0.001413
-180.5	0.000050	636	-134.2	0.000151	960	-62.6	0.000832
-193.7	0.000036	660	-157.2	0.000087	984	-83.8	0.000501
-201.8	0.000030	684	-186.2	0.000044	1008	-105.3	0.000302
-206.9	0.000027	708	-203.5	0.000029	1032	-125.2	0.000186
-211.3	0.000024	732	-209.8	0.000025	1056	-145.3	0.000115
-215.3	0.000021	756	-211.3	0.000024	1080	-168.7	0.000066
-221.2	0.000019	816	-218.3	0.000020	1104	-183.3	0.000048
-225.0	0.000017	876	-223.0	0.000018	1128	-204.7	0.000028
		936	-227.3	0.000016	1152	-209.5	0.000025
		996	-230.5	0.000015	1176	-211.6	0.000022
		1116	-236.4	0.000013	1200	-217.3	0.000021
		1236	-243.2	0.000011	1260	-224.7	0.000017
		1356	-245.9	0.000010	1320	-230.7	0.000015
					1440	-241.3	0.000012
					1560	-245.9	0.000010

TABLE 4

HYDROGEN REDUCTION OF OXYGEN SATURATED LEAD

Temperature : 700°C Orifice dia. : 0.48 cm

Flow rate (cc/min)

183.0		140.2			95.5		
EMF (mV)	Concentration (atom /)	Time (secs)	EMF (mV)	Concentration (atom /)	Time (secs)	EMF (mV)	Concentration (atom /)
119.1	0.063102	0	143.2	0.112204	0	138.4	0.100002
-103.7	0.043851	60	142.2	0.109613	60	136.8	0.095502
89.8	0.031620	90	137.4	0.097721	120	134.2	0.091204
78.9	0.023991	120	125.9	0.074130	180	131.3	0.085110
71.0	0.021384	150	119.1	0.063102	240	129.7	0.081283
69.2	0.019506	180	114.8	0.056890	300	127.7	0.077624
64.7	0.017263	210	112.5	0.053953	360	124.8	0.072443
59.8	0.015380	240	109.3	0.050122	420	120.0	0.064672
54.7	0.013652	270	106.8	0.046772	480	116.1	0.059881
52.1	0.012791	300	103.6	0.043654	540	113.2	0.054950
47.8	0.011220	330	100.2	0.040271	600	109.3	0.050122
42.2	0.010121	360	96.9	0.037150	660	104.6	0.044673
38.9	0.009333	390	93.0	0.033882	720	99.7	0.039810
35.2	0.008551	420	88.1	0.030204	780	94.0	0.035482
32.1	0.007943	450	84.3	0.027543	840	87.2	0.029510
28.3	0.007244	480	80.4	0.025120	900	79.4	0.024551
24.4	0.006207	510	78.7	0.024104	960	69.2	0.019506
20.5	0.006026	540	71.0	0.021384	1020	59.2	0.015143
18.6	0.005754	570	67.8	0.018621	1080	47.8	0.011220
16.6	0.005495	600	63.0	0.016602	1110	37.9	0.009120
12.3	0.004955	630	57.3	0.014453	1140	29.2	0.007413
3.1	0.003981	660	51.4	0.012592	1170	18.0	0.005623
-6.5	0.003162	690	44.7	0.010723	1200	5.5	0.004074
-16.2	0.002512	720	37.9	0.009120	1230	-12.3	0.002754
-25.9	0.001995	750	29.2	0.007413	1260	-28.1	0.001905
-35.6	0.001585	780	19.7	0.005916	1290	-44.6	0.001288
-45.3	0.001259	804	5.1	0.004169	1320	-56.8	0.000955

) 4 (contd.)

Flow rate (cc/min)

183.0			140.2			95.5		
e s)	EMF (mv)	Concentration (atom /)	Time (secs)	EMF (mV)	Concentration (atom /)	Time (secs)	EMF (mV)	Concentration (atom /)
	-54.9	0.001000	816	-4.6	0.003311	1350	-70.4	0.000692
	-66.5	0.000759	828	-15.1	0.002582	1380	-83.0	0.000513
	-76.2	0.000600	840	-22.0	0.002188	1410	-95.5	0.000380
	-87.7	0.000457	852	-28.1	0.001905	1440	-107.9	0.000282
	-96.4	0.000372	864	-35.6	0.001585	1470	-122.5	0.000200
	-105.0	0.000306	888	-49.1	0.001148	1500	-135.7	0.000145
	-111.8	0.000257	912	-64.5	0.000794	1530	-151.2	0.000100
	-122.5	0.000200	936	-83.8	0.000501	1560	-164.9	0.000072
	-132.1	0.000159	960	-97.3	0.000363	1590	-177.7	0.000054
	-140.8	0.000129	984	-110.9	0.000263	1620	-185.3	0.000045
	-151.2	0.000100	1008	-125.2	0.000186	1680	-195.8	0.000035
	-160.3	0.000081	1032	-139.8	0.000131	1740	-201.9	0.000030
	-171.0	0.000063	1056	-158.2	0.000083	1800	-209.6	0.000025
	-178.7	0.000052	1080	-174.7	0.000058	1860	-215.4	0.000022
	-183.2	0.000047	1104	-182.7	0.000048	1920	-219.2	0.000020
	-187.7	0.000042	1128	-187.7	0.000042	2040	-224.9	0.000017
	-193.2	0.000037	1152	-190.3	0.000040			
	-195.9	0.000035	1182	-195.9	0.000035			
	-201.1	0.000031	1212	-198.6	0.000033			
	-203.7	0.000029	1242	-201.8	0.000030			
	-205.7	0.000028	1272	-203.7	0.000029			
	-207.6	0.000026	1332	-207.6	0.000026			
	-211.3	0.000024	1392	-211.2	0.000024			
	-211.9	0.000024	1452	-213.5	0.000023			
	-214.6	0.000022	1512	-215.3	0.000022			
	-215.4	0.000022	1632	-219.3	0.000020			
	-217.2	0.000021						
	-221.1	0.000019						
	-223.1	0.000018						
	-224.8	0.000017						
	-227.0	0.000017						
	-228.8	0.000016						
	-229.1	0.000016						

TABLE 5

HYDROGEN REDUCTION OF OXYGEN SATURATED LEAD

Temperature : 750°C Orifice dia. : 0.48 cm

Flow rate (cc/min)

181.8			132.8			84.3		
Time (secs)	EMF (mV)	Concentration (atom /)	Time (secs)	EMF (mV)	Concentration (atom /)	Time (secs)	EMF (mV)	Concentration (atom /)
0	135.5	0.226504	0	124.8	0.177801	0	135.5	0.226504
30	122.6	0.169013	60	116.6	0.147910	60	128.8	0.194999
60	111.6	0.131804	120	108.0	0.121604	120	123.1	0.170998
90	99.4	0.100013	180	99.4	0.100013	180	117.7	0.151402
20	89.3	0.079430	240	89.3	0.079430	240	109.5	0.125901
50	79.1	0.063101	270	82.2	0.067609	300	101.4	0.104697
80	69.0	0.050119	300	76.1	0.058881	360	93.4	0.087102
10	59.0	0.039812	330	69.0	0.050119	420	85.2	0.072438
40	50.7	0.033109	360	62.9	0.043648	480	78.1	0.061662
70	41.6	0.026921	390	56.8	0.038022	540	65.9	0.046769
00	33.4	0.022388	420	51.7	0.033879	600	57.8	0.038901
30	18.2	0.015852	450	46.7	0.030201	660	47.7	0.030902
60	4.0	0.011479	480	40.5	0.026302	720	37.5	0.024551
72	-9.2	0.008511	510	36.5	0.023989	780	27.4	0.019498
84	-21.7	0.006339	540	31.4	0.021382	840	13.1	0.014130
96	-32.5	0.005012	570	25.4	0.018619	900	-2.1	0.009999
08	-44.7	0.003802	600	18.2	0.015852	924	-10.2	0.008318
20	-50.8	0.003311	630	12.1	0.013801	948	-21.4	0.006457
32	-57.9	0.002818	660	0.4	0.010468	960	-30.5	0.005248
44	-67.1	0.002291	690	-10.2	0.008318	972	-36.6	0.004571
56	-75.1	0.001905	720	-21.7	0.006339	984	-42.7	0.003981
68	-93.3	0.001257	744	-34.6	0.004786	996	-49.9	0.003388
80	-105.7	0.000955	756	-44.7	0.003802	1008	-52.9	0.003162
92	-111.8	0.000832	768	-56.9	0.002884	1020	-57.9	0.002818
04	-124.0	0.000631	780	-67.1	0.002291	1032	-63.0	0.002512
16	-144.3	0.000398	792	-76.0	0.001862	1044	-69.1	0.002188
28	-150.2	0.000331	804	-87.3	0.001445	1050	-72.1	0.002042
40	-161.7	0.000270	816	-93.3	0.001257	1062	-76.0	0.001862
52	-178.7	0.000182	828	-99.5	0.001096	1074	-81.2	0.001660

able 5 (contd.)

Flow rate (cc/min)								
181.8			132.8			84.3		
Time (secs)	EMF (mV)	Concentration (atom /)	Time (secs)	EMF (mV)	Concentration (atom /)	Time (secs)	EMF (mV)	Concentration (atom /)
564	-184.8	0.000159	840	-105.7	0.000955	1086	-86.4	0.001479
576	-193.9	0.000129	852	-111.8	0.000832	1098	-90.3	0.001349
588	-205.0	0.000100	864	-119.8	0.000692	1110	-94.5	0.001230
600	-215.2	0.000079	876	-127.8	0.000574	1122	-99.5	0.001096
612	-226.6	0.000060	888	-138.0	0.000457	1128	-101.6	0.001047
624	-237.7	0.000048	900	-146.3	0.000380	1158	-110.8	0.000851
648	-240.5	0.000045	912	-156.3	0.000302	1188	-126.0	0.000562
678	-245.8	0.000040	924	-166.6	0.000240	1218	-140.2	0.000437
708	-249.7	0.000036	936	-176.6	0.000191	1248	-160.3	0.000275
768	-253.6	0.000033	948	-184.8	0.000159	1260	-164.6	0.000251
826	-254.9	0.000032	960	-190.9	0.000138	1272	-171.6	0.000214
948	-257.7	0.000030	972	-199.2	0.000115	1284	-175.8	0.000195
			984	-207.2	0.000096	1296	-180.7	0.000174
			996	-215.2	0.000079	1308	-189.0	0.000145
			1008	-221.3	0.000070	1320	-193.9	0.000129
			1020	-222.3	0.000068	1332	-199.8	0.000112
			1032	-225.4	0.000063	1344	-203.9	0.000102
			1044	-229.3	0.000058	1356	-207.2	0.000096
			1056	-231.0	0.000055	1380	-209.1	0.000091
			1080	-235.4	0.000050	1392	-213.3	0.000083
			1104	-239.6	0.000046	1404	-223.3	0.000068
			1134	-242.8	0.000043	1416	-226.6	0.000060
			1164	-245.8	0.000040	1428	-231.0	0.000055
			1194	-249.7	0.000036	1440	-235.4	0.000050
			1224	-251.9	0.000035	1452	-242.7	0.000043
			1284	-253.6	0.000033	1464	-247.7	0.000038
			1344	-257.1	0.000031	1476	-250.8	0.000035
						1488	-252.7	0.000034
						1500	-254.9	0.000032
						1512	-255.8	0.000032
						1536	-257.1	0.000031
						1560	-257.3	0.000031
						1584	-257.5	0.000030

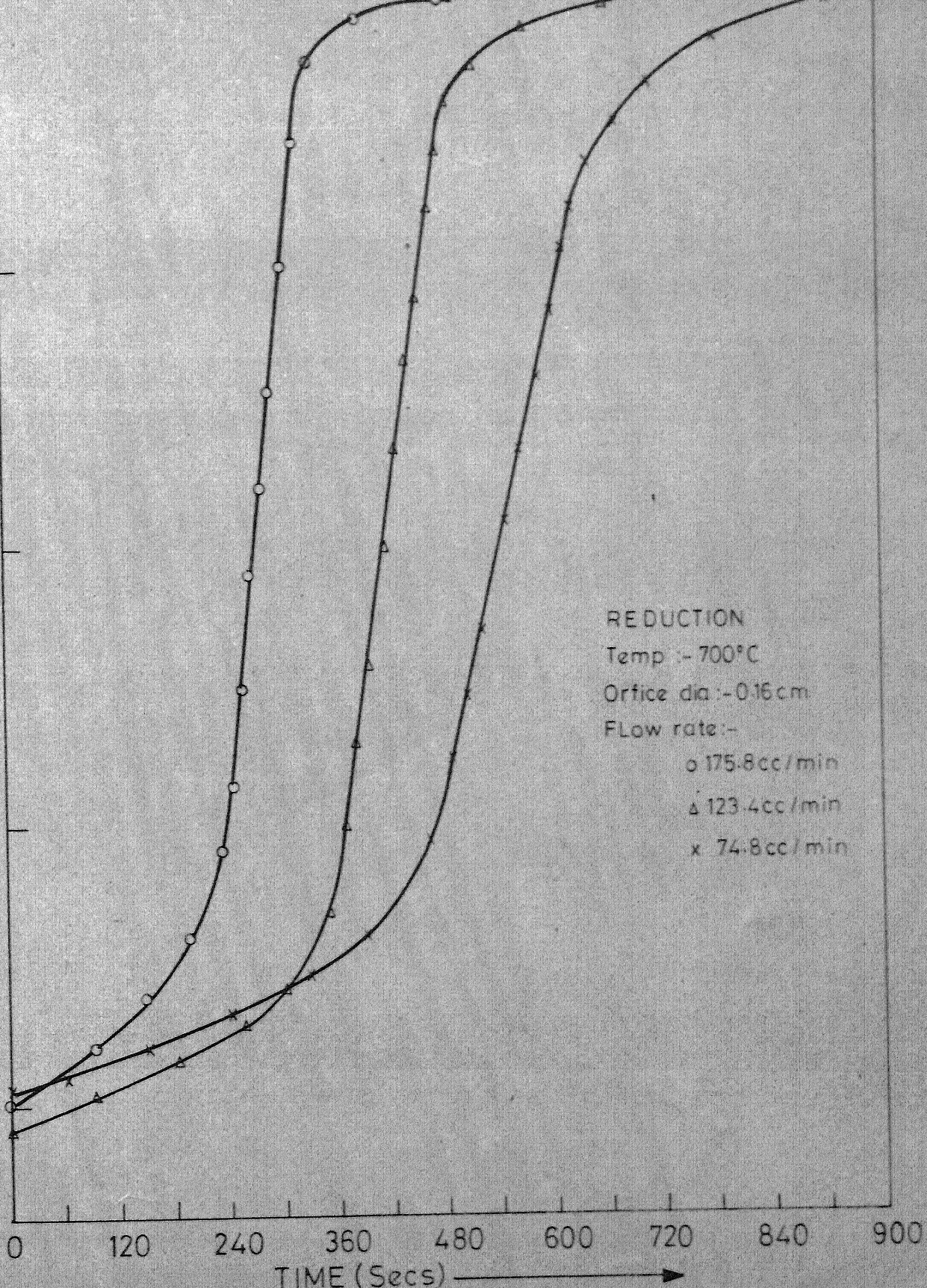


FIG. 5 PLOTS OF LOG (C) VS TIME FOR HYDROGEN REDUCTION

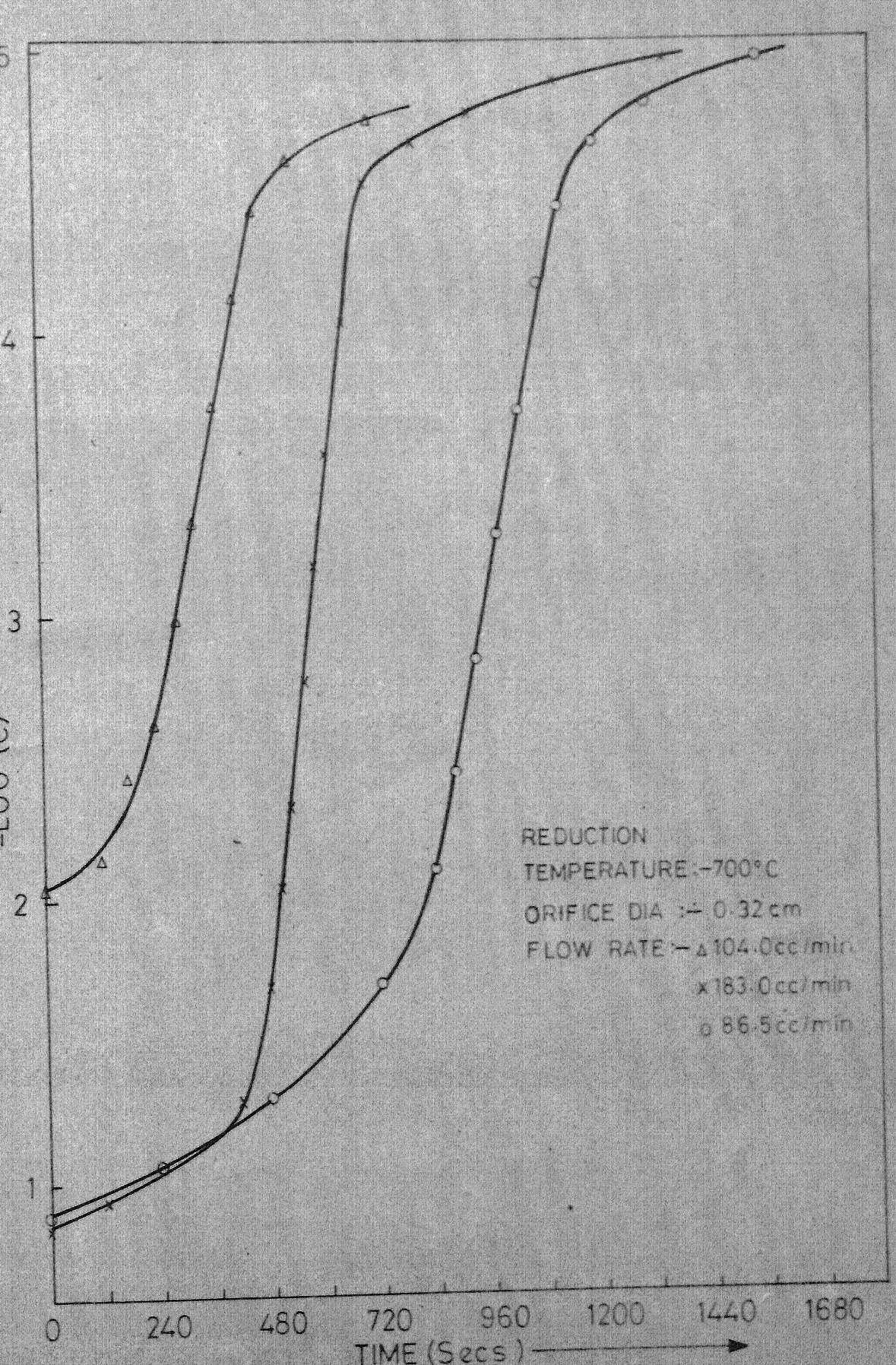


FIG. 6 PLOTS OF LOG (C) VS TIME FOR HYDROGEN REDUCTION

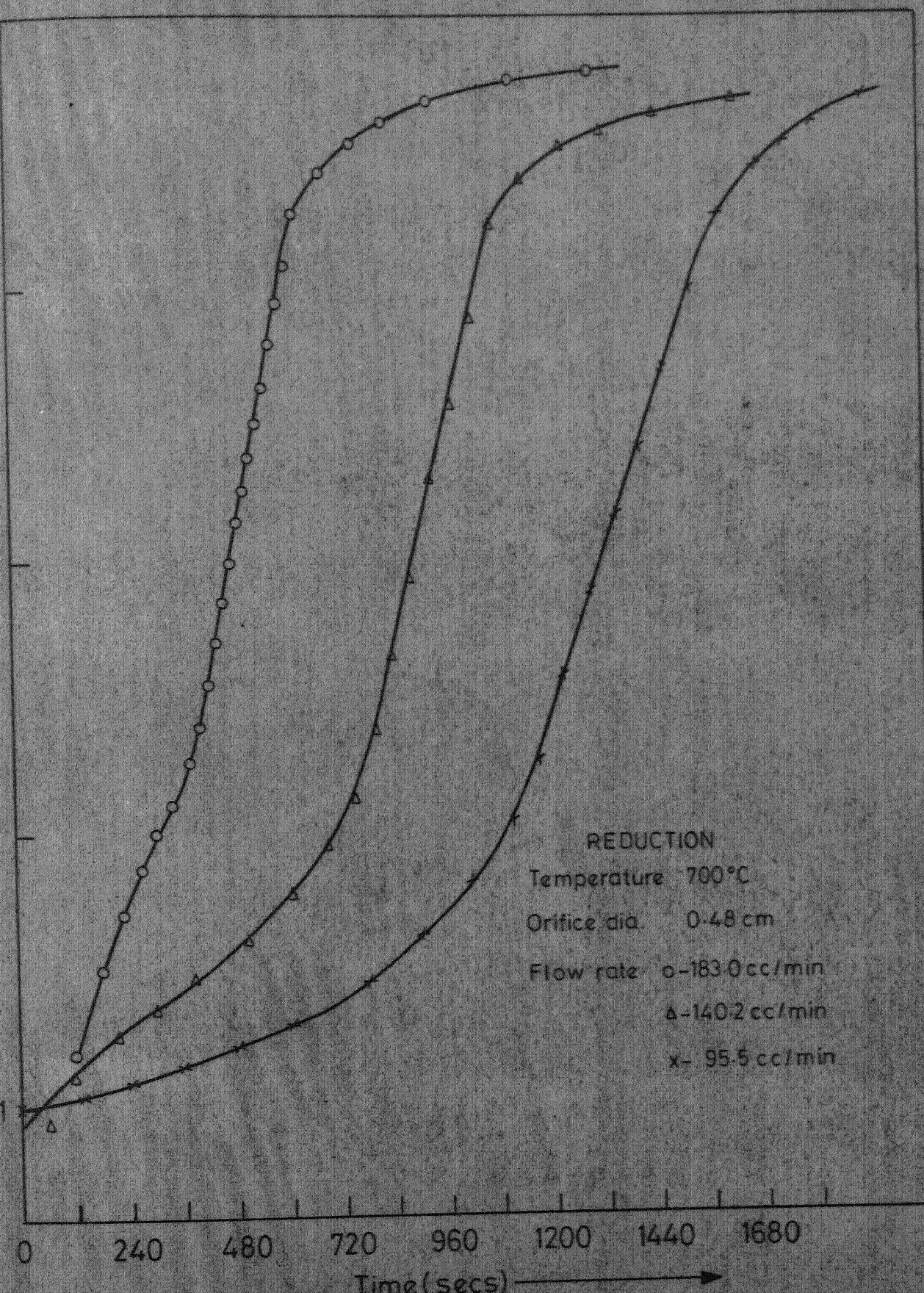


FIG. 7 PLOTS OF LOG (C) VS TIME FOR HYDROGEN REDUCTION.

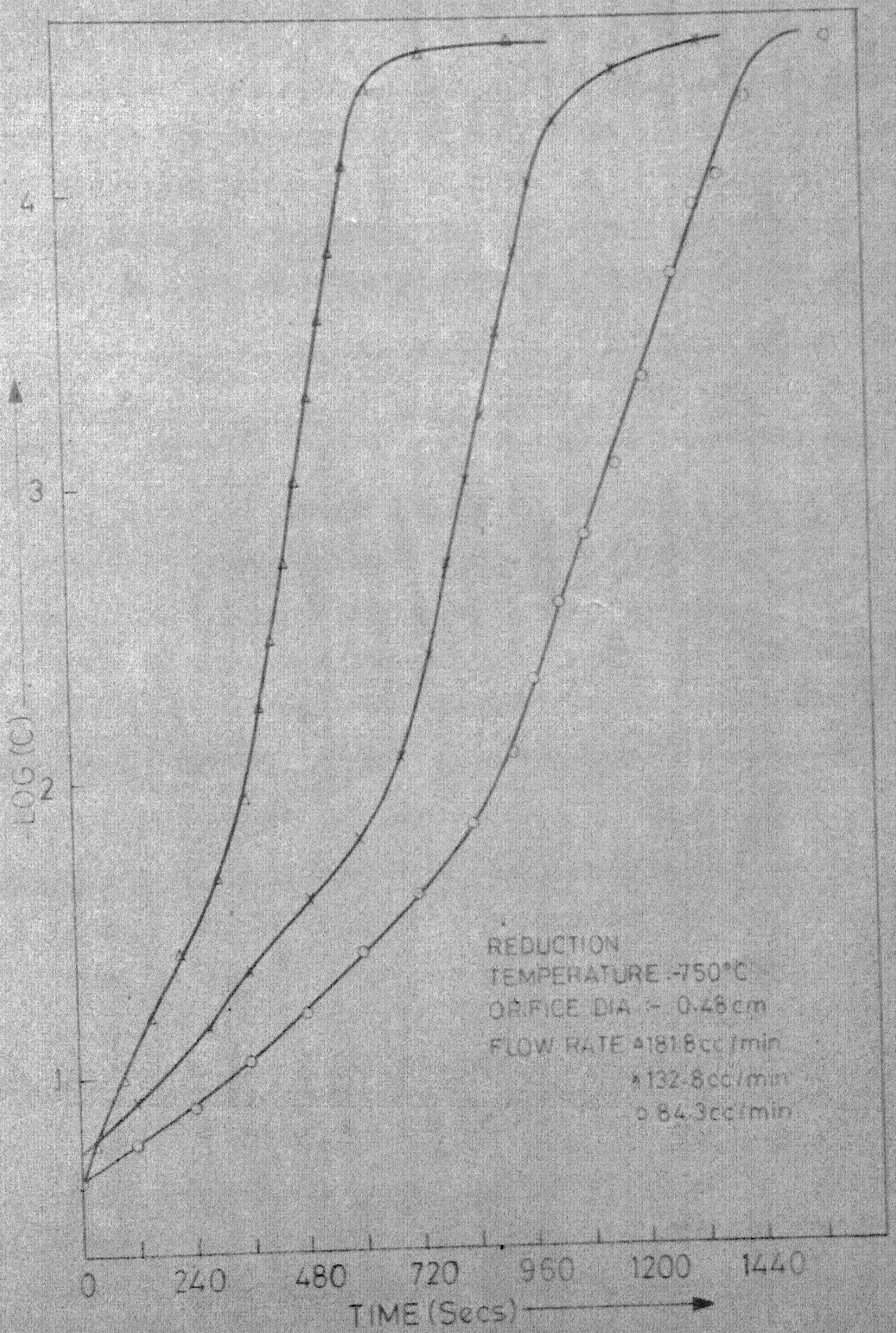


FIG 8 PLOTS OF LOG (C) Vs TIME FOR HYDROGEN REDUCTION.

concentration decreases to a value which is the same order of magnitude as the concentration at the interface, the same driving force for oxygen transport can no longer be sustained as a result of which the rate of transport of oxygen to the interface decreases a hence the rate of removal of oxygen decreases.

The slopes of the linear regions of the plots of log (C) against time give $-\frac{1}{V_m}\left[\frac{D}{\delta}A_s + \frac{3K_L F \tau_r}{r_b}\right]$ for spherical bubbles and $-\frac{1}{V_m}\left[\frac{D}{\delta}A_s + \frac{3.016\ K_L F \tau_r}{r_b}\right]$ for spherical-cap bubbles. Now if these slopes are plotted against the respective flow rates, then the slopes of these plots will give $-\frac{3K_L \tau_r}{V_m r_b}$ and $-\frac{3.016\ K_L \tau_r}{V_m r_b}$ for spherical and spherical-cap bubbles respectively. The intercepts of these plots should give $-\frac{D A_s}{V_m \delta}$. The slopes of the plots of log (C) versus time have been plotted against flow rate in Figures 9 and 10. K_L and $\frac{D}{\delta}$ values have been calculated and are given in Table 11.

Oxidation runs As in the case of the reduction runs the changing e.m.f. was converted to oxygen concentrations (Tables 6 - 10) and from them, log (C_s-C) values were calculated, the concentrations at the interface C_s being calculated using Alcock and Belford's[41] equation

$$\log_{10}(\text{N Pb.at \% O}) = \frac{-2240}{T} + 4.55 \qquad (30)$$

For each run log (C_s-C) was plotted against flow rate. These plots are shown in Figures 11-15. Once again the same trend as observed in the hydrogen reduction runs was seen, that is, the rate of oxygen dissolution increased initially, attained a constant value and then near the end of each run decreased. In the intermediate region where the rate of dissolution of oxygen in the

A 23389

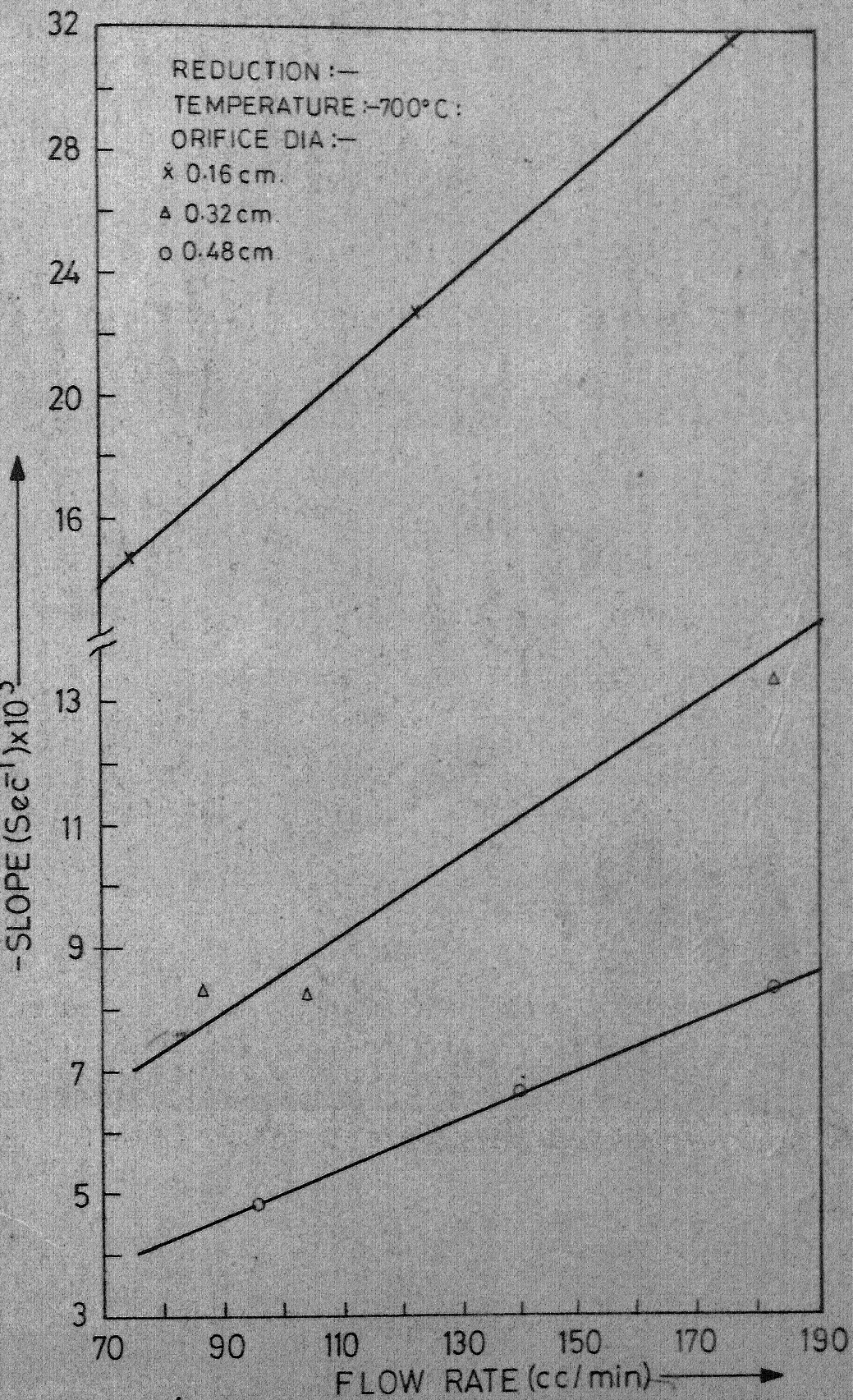


FIG.9 PLOTS OF SLOPES OF LOG (C) VS TIME PLOTS VERSUS FLOW RATE FOR HYDROGEN REDUCTION.

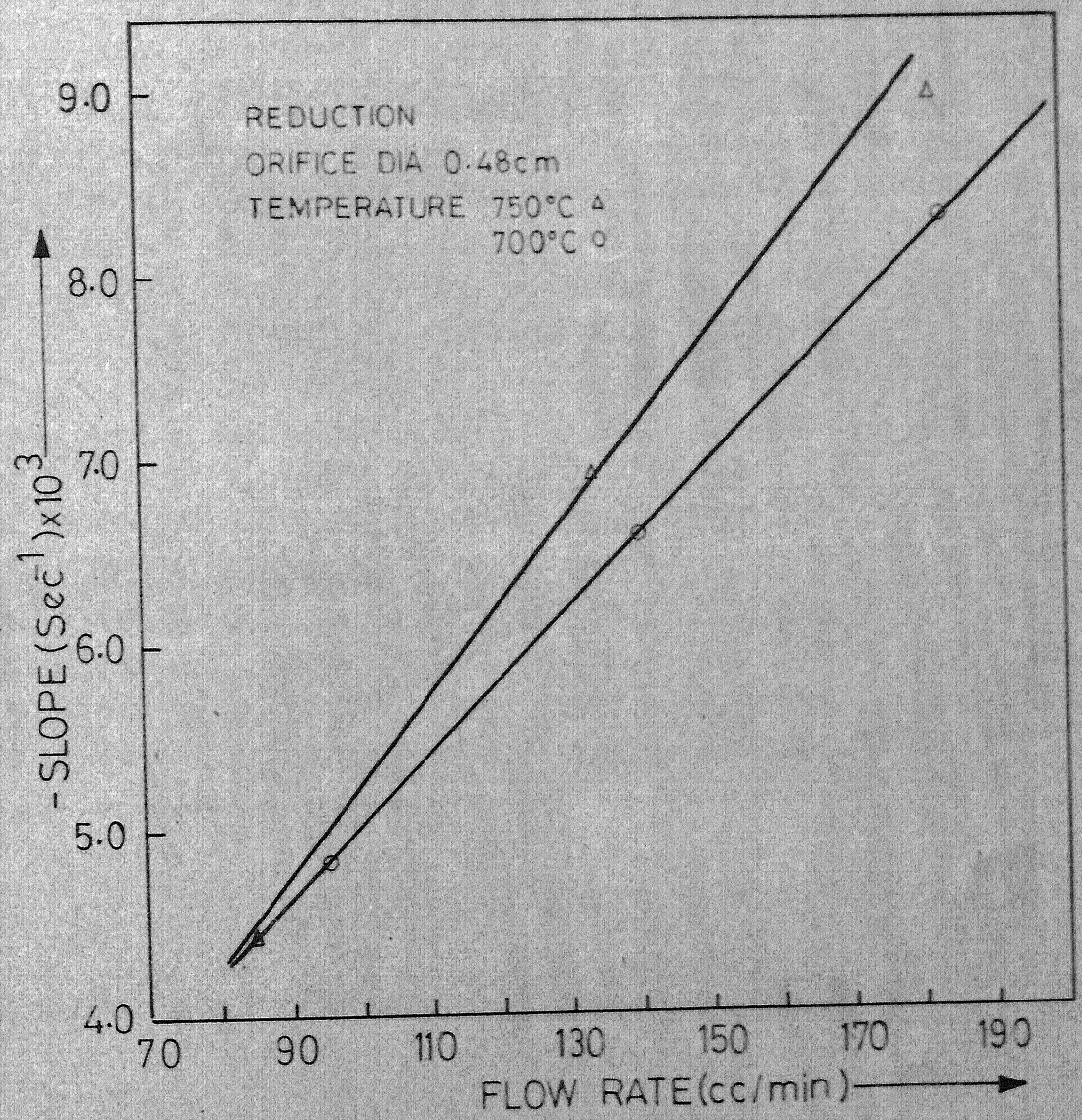


FIG.10. PLOTS OF SLOPES OF LOG (C) VS TIME PLOTS VERSUS FLOW RATE FOR HYDROGEN REDUCTION.

TABLE 6

OXIDATION OF LIQUID LEAD BY ARGON-OXYGEN MIXTURE

Temperature : 700°C Orifice dia. : 0.16 cm

Flow rate (cc/min)

153.7			121.2			76.7		
Time (secs)	EMF (mV)	Concentration (atom /)	Time (secs)	EMF (mV)	Concentration (atom /)	Time (secs)	EMF (mV)	Concentration (atom /)
180	-91.8	0.000414	186	-23.9	0.003412	183	-162.3	0.000077
183	-51.3	0.001086	189	-3.3	0.003412	186	-66.8	0.000750
186	-12.4	0.002751	192	10.3	0.004725	192	-12.4	0.002751
189	7.3	0.004398	195	28.6	0.007315	198	15.7	0.005377
192	26.8	0.006994	198	42.2	0.010172	201	30.4	0.007635
195	42.5	0.010172	201	56.4	0.014195	204	45.0	0.010799
198	59.9	0.015409	204	72.3	0.020735	207	60.7	0.015711
201	75.7	0.022462	207	95.7	0.036217	210	73.3	0.020735
204	100.3	0.040454	210	108.3	0.048898	216	104.1	0.044294
207	113.5	0.055419	213	116.5	0.059523	222	116.2	0.059121
210	121.6	0.067184	216	122.6	0.068813	228	124.2	0.071454
213	127.9	0.078065	219	127.9	0.078065	234	129.8	0.081750
216	131.9	0.085798	222	131.6	0.085236			

TABLE 7

OXIDATION OF LIQUID LEAD BY ARGON-OXYGEN MIXTURE

Temperature : 700°C Orifice dia. : 0.32 cm

Flow rate (cc/min)

166.9			135.1			76.6		
Time (secs)	EMF (mV)	Concentration (Atom /)	Time (secs)	EMF (mV)	Concentration (atom /)	Time (secs)	EMF (mV)	Concentration (atom /)
228	-162.3	0.000077	252	-23.9	0.002087	240	-162.3	0.000077
234	-135.9	0.000144	258	10.3	0.004725	246	-91.8	0.000414
240	-51.3	0.001086	264	32.1	0.007955	252	-51.3	0.001086
246	-12.4	0.002751	270	52.6	0.012970	258	-23.9	0.002087
252	7.3	0.004398	276	82.4	0.026400	264	-3.3	0.003412
258	32.1	0.007955	282	96.0	0.036471	270	7.3	0.004398
264	57.3	0.014500	288	106.3	0.046622	276	7.0	0.004365
270	87.3	0.029676	294	113.5	0.055419	282	20.3	0.006026
276	101.3	0.041427	300	118.9	0.063058	288	33.8	0.008274
282	112.2	0.053724	306	123.9	0.070933	294	45.0	0.010799
288	118.7	0.062672	312	127.2	0.076791	300	54.6	0.013584
294	124.2	0.071454	318	130.7	0.083517	306	62.3	0.016312
300	128.6	0.079316				312	79.7	0.024728
306	132.4	0.086908				324	97.4	0.037731
						336	108.7	0.049347
						348	116.8	0.059923
						360	122.7	0.068992
						372	127.7	0.077749

TABLE 8

OXIDATION OF LIQUID LEAD BY ARGON-OXYGEN MIXTURE

Temperature : 700°C Orifice dia. : 0.48 cm

Flow rate (cc/min)

151.1			135.1			78.2		
Time (secs)	EMF (mV)	Concentration (atom /)	Time (secs)	EMF (mV)	Concentration (atom /)	Time (secs)	EMF (mV)	Concentration (atom /)
528	-66.8	0.000750	528	-58.0	0.000941	528	-40.1	0.001420
534	-51.3	0.001086	534	-45.1	0.001281	534	-23.9	0.002087
540	-31.2	0.001754	540	-14-9	0.002630	540	-12.4	0.002751
546	-17.7	0.002420	546	2.4	0.003967	546	-3.3	0.003412
552	-3.3	0.003412	552	14.4	0.005292	558	20.5	0.006026
558	15.7	0.005377	558	23.7	0.006605	564	18.2	0.005702
564	33.8	0.008274	564	43.1	0.010472	570	28.6	0.007315
570	43.7	0.010485	570	56.0	0.014233	576	39.8	0.009542
576	59.9	0.015409	576	68.3	0.019089	582	51.6	0.012662
582	69.9	0.019571	582	77.5	0.023769	588	61.5	0.016012
588	80.2	0.025009	588	90.1	0.032093	594	69.9	0.019571
594	93.3	0.034165	600	102.9	0.043549	600	80.2	0.025009
606	111.2	0.052432	606	109.2	0.050553	608	88.1	0.030213
612	117.4	0.060718	612	113.0	0.055990	612	95.4	0.035963
618	122.1	0.067912	618	115.5	0.058757	618	102.3	0.042392
624	125.8	0.074538	624	116.8	0.060597	624	108.3	0.048898
630	126.9	0.076145	630	118.3	0.062795	630	112.9	0.054576
636	127.9	0.078065	660	123.5	0.071229	636	115.4	0.057904
642	129.0	0.080239	690	125.5	0.074705	642	119.2	0.063442
			720	127.5	0.078349	648	121.6	0.067184
						654	123.8	0.070758
						660	124.8	0.072485
						666	125.6	0.073857
						678	126.7	0.075820

TABLE 9

OXIDATION OF LIQUID LEAD BY ARGON-OXYGEN MIXTURE

Temperature : 750°C Orifice dia. : 0.48 cm

Flow rate (cc/min)

153.4			105.0			80.1		
Time (secs)	EMF (mV)	Concentration (atom /)	Time (secs)	EMF (mV)	Concentration (atom /)	Time (secs)	EMF (mV)	Concentration (atom /)
558	-19.8	0.004839	540	-116.0	0.000546	540	-116.0	0.000546
564	1.6	0.007864	546	-40.8	0.003008	546	-63.9	0.001780
570	22.5	0.012631	552	-25.7	0.004230	552	-50.8	0.002395
576	57.7	0.020088	558	-10.0	0.006053	564	-14.6	0.005447
582	89.4	0.057727	564	20.4	0.012040	570	-1.9	0.007262
588	105.4	0.082865	570	61.0	0.030297	576	7.8	0.009064
594	113.7	0.100027	576	83.4	0.050301	588	22.5	0.012631
600	120.6	0.117014	582	94.6	0.064902	594	30.0	0.014982
606	126.8	0.134789	588	102.8	0.078089	600	40.6	0.019045
612	129.5	0.143171	600	117.2	0.108376	606	47.9	0.022475
618	130.5	0.146602	612	124.5	0.127813	612	57.7	0.028088
			618	127.0	0.135406	618	77.7	0.044172
			624	127.6	0.137239	624	88.3	0.056262
			636	128.6	0.140240	630	97.7	0.069549
						636	103.7	0.079839
						648	114.4	0.101577
						660	121.8	0.120132
						666	124.7	0.128462
						672	126.8	0.134789
						684	127.2	0.136020

TABLE 10

OXIDATION OF LIQUID LEAD BY ARGON-OXYGEN MIXTURE

Temperature : 650.5°C Orifice dia. : 0.48 cm

Flow rate (cc/min)

106.1			161.2			86.8		
Time (secs)	EMF (mV)	Concentration (atom /)	Time (secs)	EMF (mV)	Concentration (atom /)	Time (secs)	EMF (mV)	Concentration (atom /)
726	-78.0	0.000237	726	-72.6	0.000278	726	-72.6	0.000278
738	-72.5	0.000271	738	-53.1	0.000455	732	-67.9	0.000314
750	-42.2	0.000582	762	-22.4	0.000982	738	-40.0	0.000631
762	2.3	0.001778	768	-10.3	0.001331	744	-15.9	0.001156
774	51.0	0.006055	780	25.0	0.003223	750	2.9	0.001852
786	77.3	0.011716	786	38.9	0.004570	756	20.5	0.002883
798	90.3	0.016238	792	59.5	0.007670	762	38.9	0.004570
810	96.6	0.019029	798	74.8	0.011243	768	49.0	0.005892
822	99.7	0.020565	804	84.9	0.014493	774	64.9	0.008778
834	101.8	0.021689	810	89.7	0.016536	780	73.1	0.010790
894	106.0	0.024105	816	96.6	0.019465	788	81.6	0.013331
			828	103.2	0.022932	792	87.2	0.015350
			834	105.9	0.024526	798	91.0	0.016892
						804	95.3	0.018798
						810	96.1	0.019199
						816	100.2	0.021289
						828	102.5	0.022557

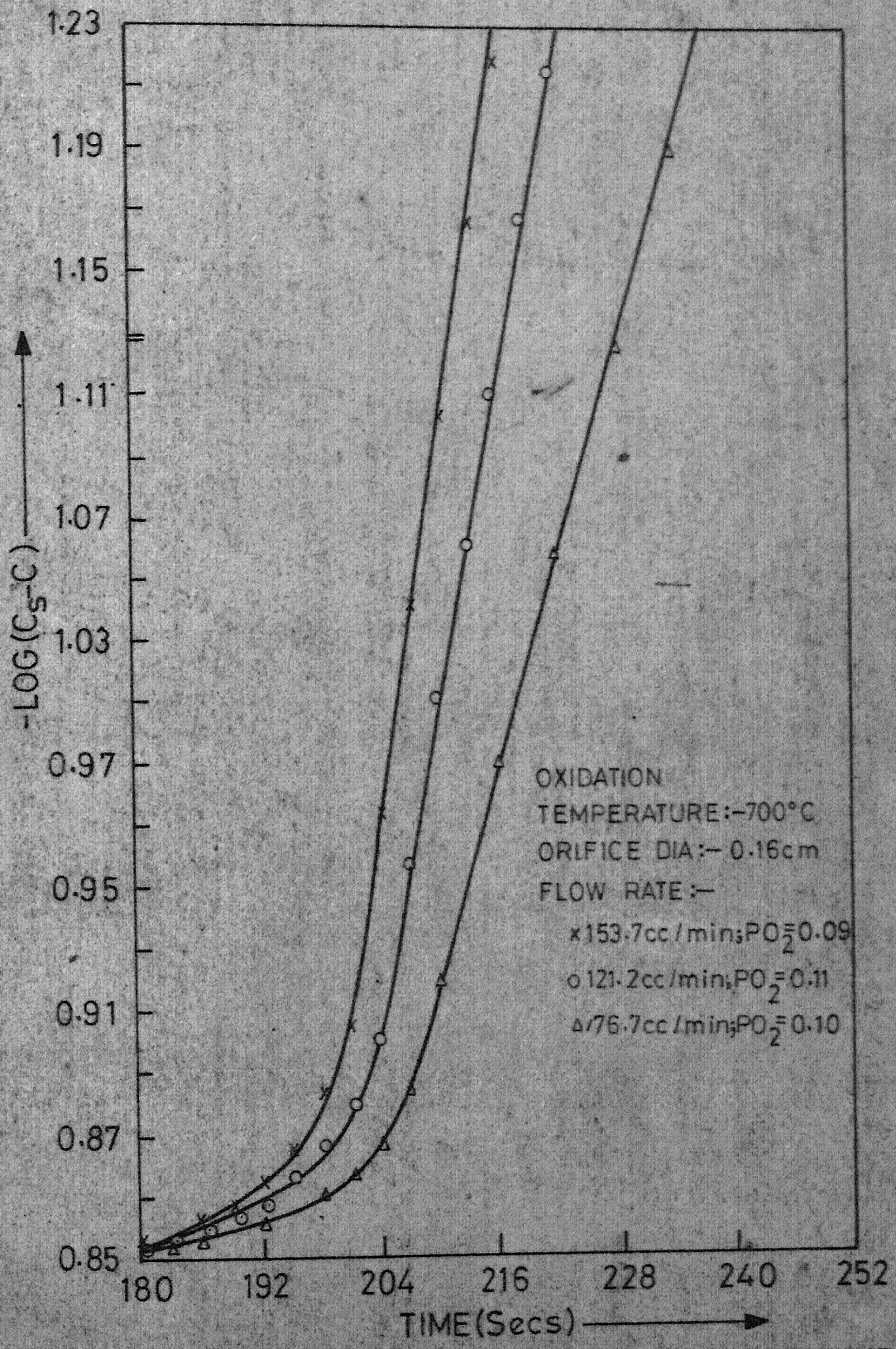


FIG.11 PLOTS OF LOG(Cs-C) VS TIME FOR OXIDATION.

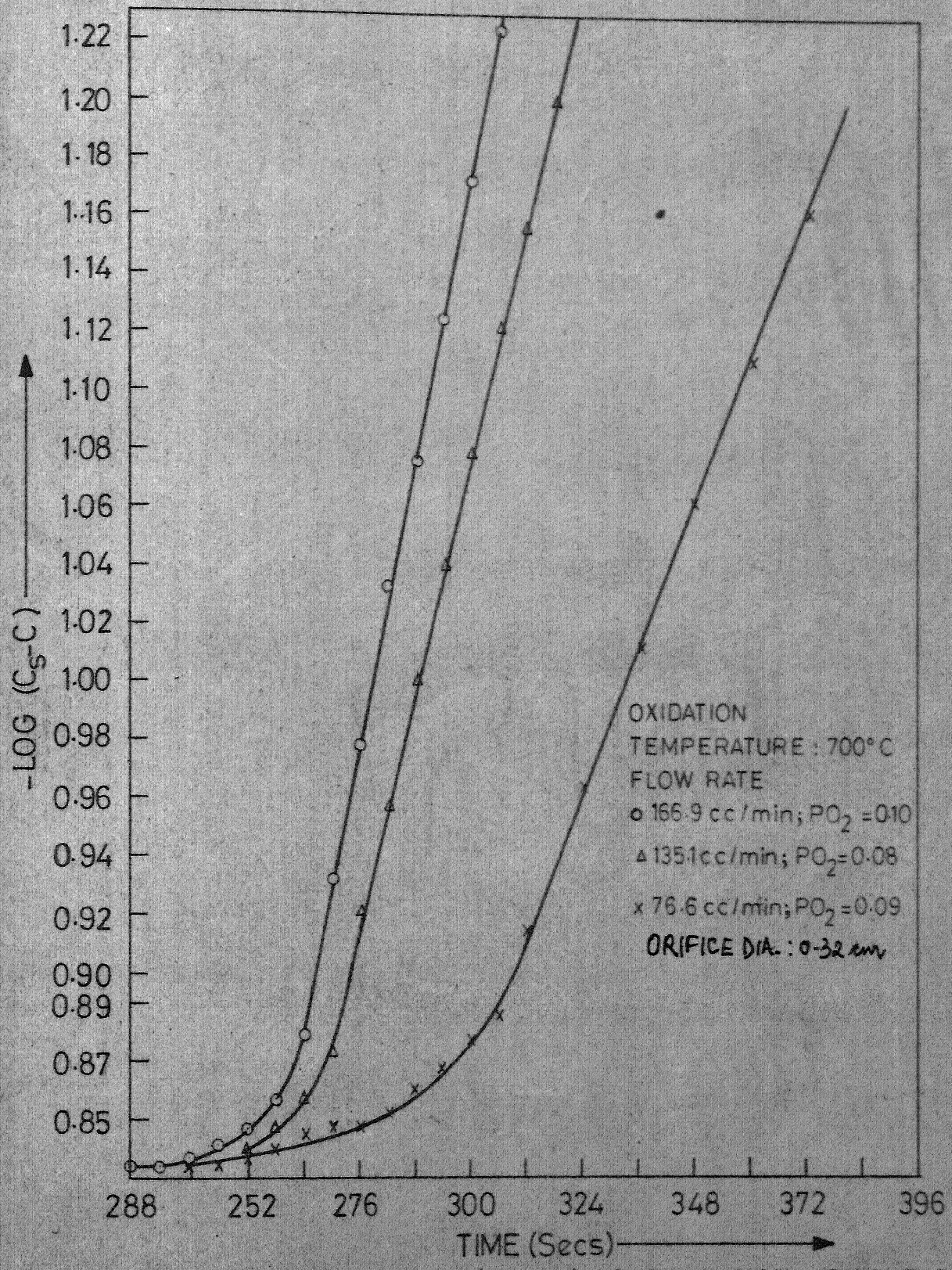


FIG.12. PLOTS OF LOG (C_s-C) VS. TIME FOR OXIDATION.

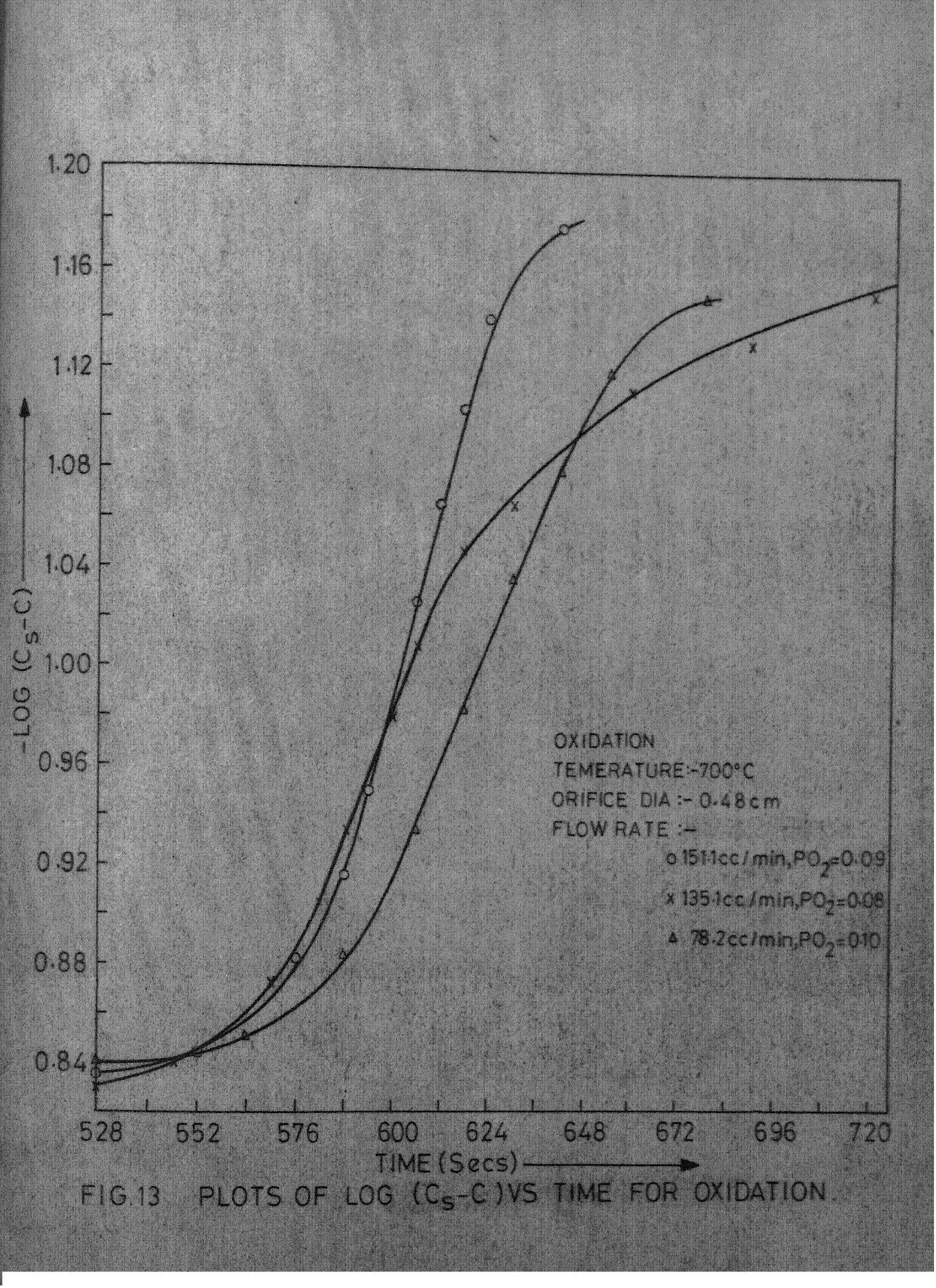


FIG.13 PLOTS OF LOG (C_s-C) VS TIME FOR OXIDATION.

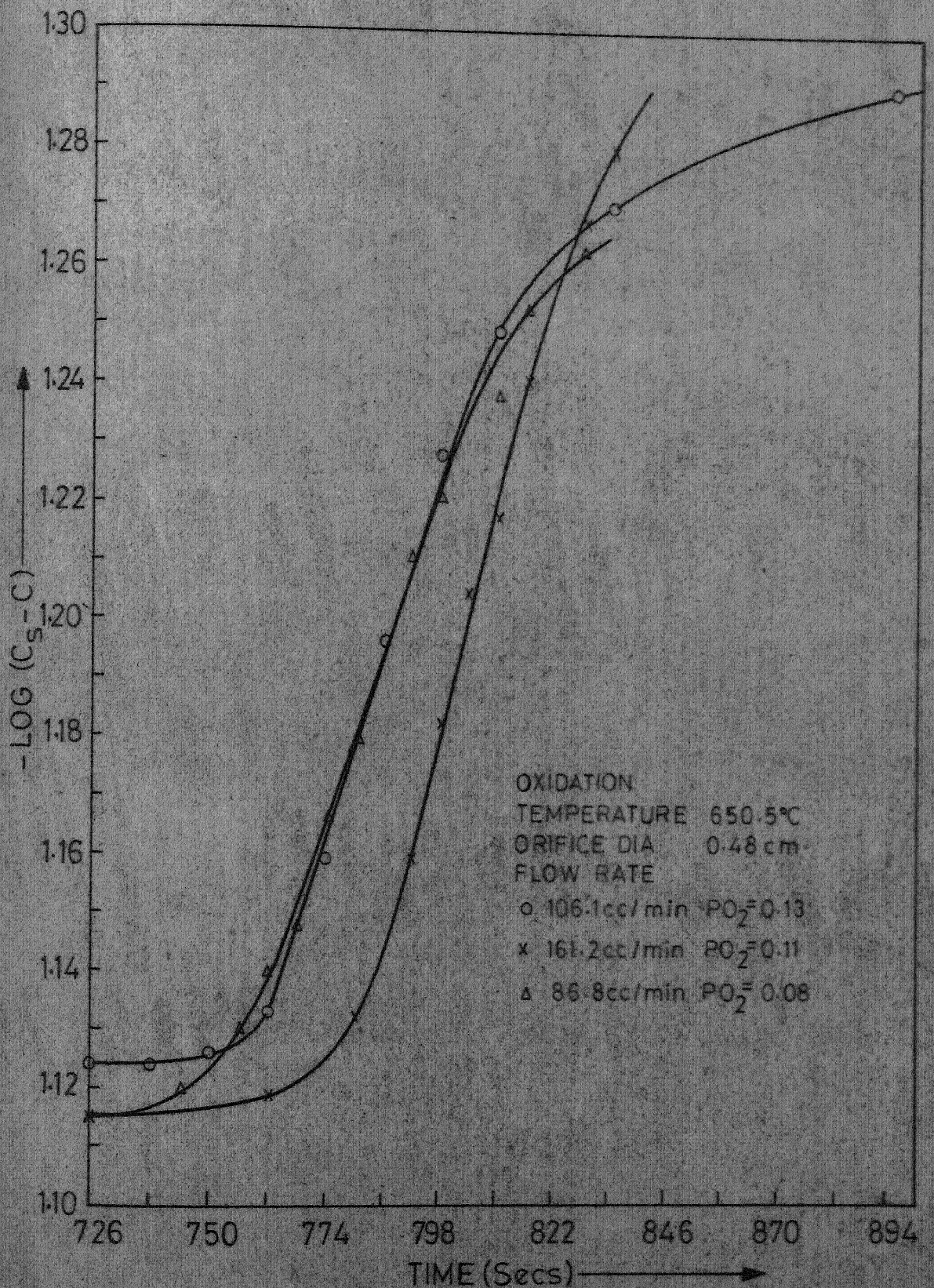


FIG. 14. PLOTS OF LOG (C_s-C) VS TIME FOR OXIDATION.

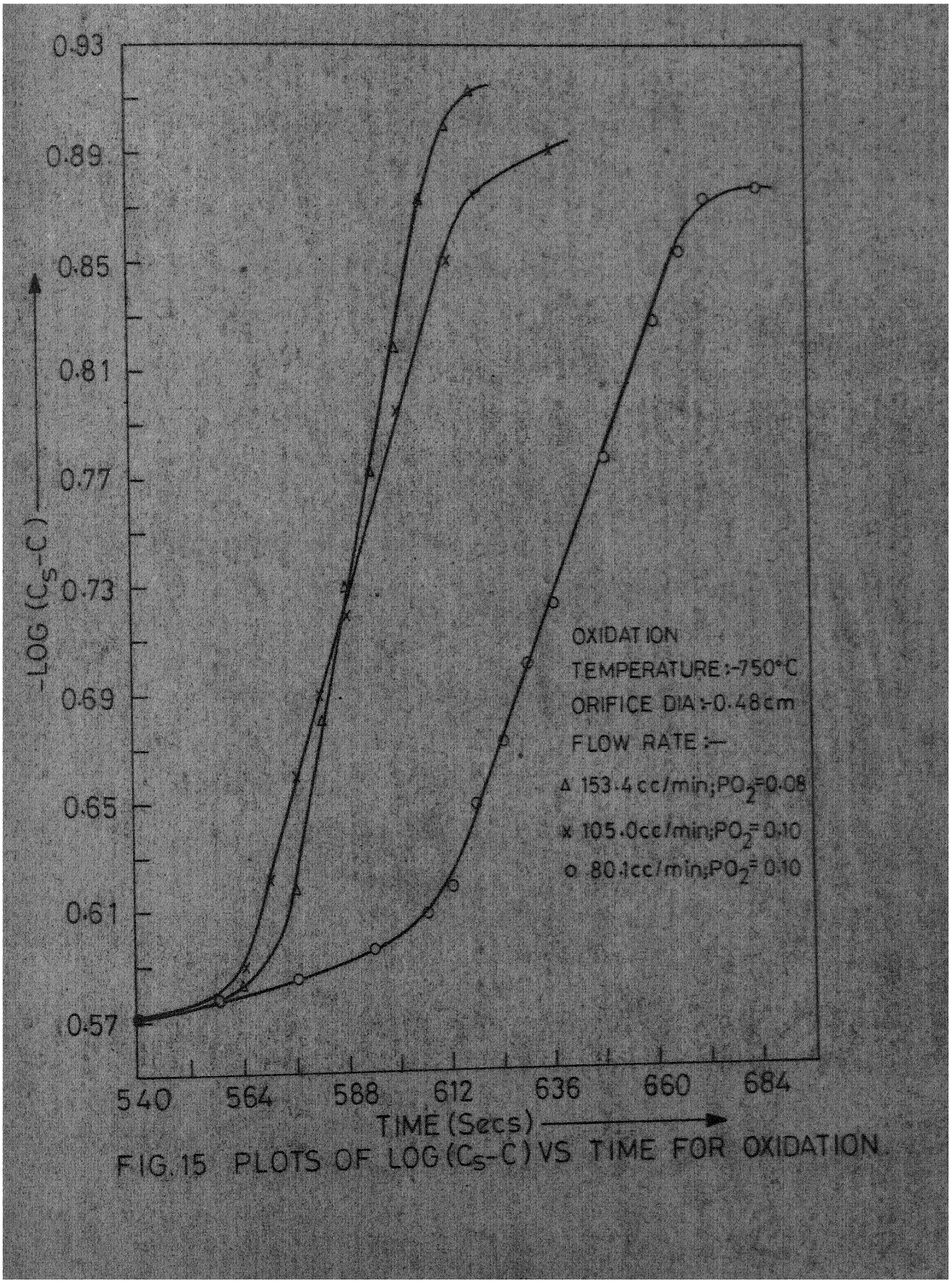


FIG. 15 PLOTS OF LOG $(C_s - C)$ VS TIME FOR OXIDATION.

molten lead is constant, equations (18) and (22) hold good and the rate controlling step is the transport of oxygen in liquid lead.

The slopes of the linear regions of the plots of $\log (C_s - C)$ against time give $-\frac{1}{V_m}\left[\frac{D}{\delta} A_s + \frac{\pi K_L \tilde{r}^2}{r_b}\right]$ for spherical bubbles and $-\frac{1}{V_m}\left[\frac{D}{\delta} A_s + \frac{3.016\, K_L \tilde{r}^2}{r_b}\right]$ for spherical-cap bubbles. As in the case of the hydrogen reduction runs, these slopes are plotted against the respective flow rates and the slopes of these plots give $-\frac{\pi K_L \tilde{r}}{V_m r_b}$ and $-\frac{3.016\, K_L \tilde{r}}{V_m r_b}$ for spherical and spherical-cap bubbles, respectively. The intercepts of these plots should give $-\frac{D A_s}{V_m \delta}$. The slopes of the plots of $\log (C_s - C)$ versus time have been plotted against flow rate in Figures 16 and 17. K_L and $\frac{D}{\delta}$ values have again been calculated and are given in Table 11.

From Table 11 it can be seen that for the same temperature and orifice diameter, there is good agreement between the values of K_L calculated from both oxidation as well as reduction runs. The agreement between the D/δ values is, however, not so good. This may be attributed to the uncertainty in the free surface of the liquid lead, which is constantly rippled by the bursting of bubbles.

Workers studying bubble-liquid interaction in room temperature aqueous liquids have found the mass transfer coefficient K_L to be dependent on the bubble diameter. To ascertain whether this was the case in bubble-liquid metal interaction also, K_L has been plotted against bubble radius

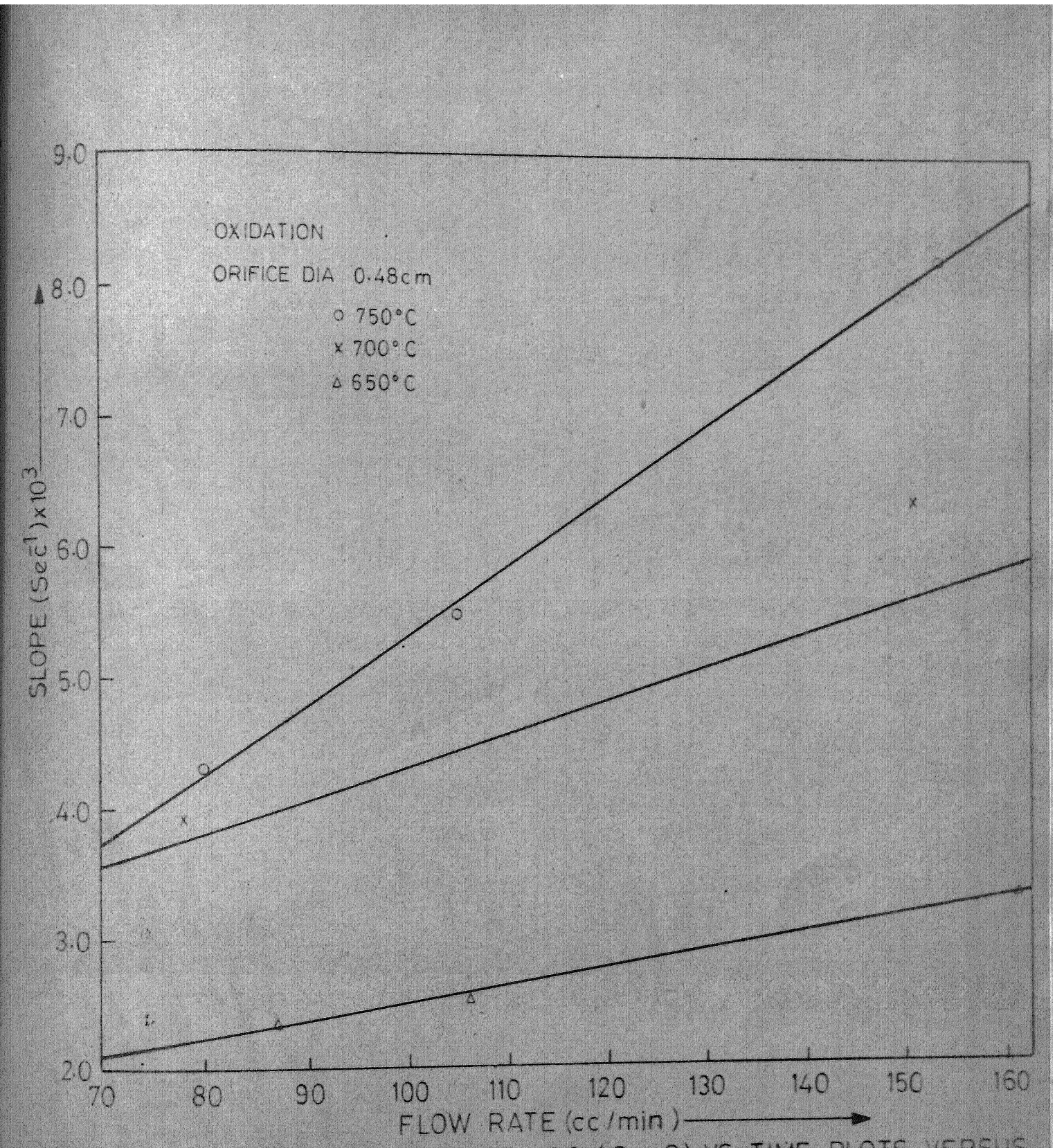


FIG. 16. PLOTS OF SLOPES OF LOG (C_s - C) VS TIME PLOTS VERSUS FLOW RATE FOR OXIDATION.

TABLE 11

CALCULATED VALUES OF MASS TRANSFER COEFFICIENTS, K_L, ACROSS BUBBLE-METAL INTERFACE, AND $\frac{D}{\delta}$, ACROSS THE FREE SURFACE AND VALUES OF BOUNDARY LAYER THICKNESS δ.

Temperature (°C)	Orifice dia. (cm)	K_L (cm/sec) (Bubble-metal interface)		D/δ (cm/sec) (free surface)		δ (cm)	
		Oxidation	Reduction	Oxidation	Reduction	Oxidation	Reduction
700	0.16	0.04709	0.04526	0.008248	0.006649	0.007079	0.008782
700	0.32	0.03352	0.04455	0.002412	0.008130	0.024100	0.007183
700	0.48	0.01453	0.02252	0.006708	0.004211	0.008706	0.013870
650.5	0.48	0.00771	—	0.004308	—	0.011410	—
750	0.48	0.03073	0.02681	0.000289	0.002055	0.236100	0.033230

as shown in Figure 18. It can be seen that the mass transfer coefficient decreases with increasing bubble size, a trend which is similar to that observed in room temperature aqueous liquids. The bold lines in Figure 18 represent Higbie's model[43] and Lochiel and Calderbank's correlation[8] for spherical bubbles. The black dots represent values of K_L calculated from Baird and Davidson correlation[15] and Lochiel and Calderbank correlation[8] for spherical-cap bubbles having an equivalent bubble radius of 0.48 cm. It can be seen that the results obtained in this work agree reasonably well with Lochiel and Calderbank correlations[8] both for spherical as well as spherical-cap bubbles.

The mass transfer coefficient K_L has also been plotted against temperature as shown in Figure 19. It is seen that K_L increases with increasing temperature. This is to be expected since essentially K_L is the diffusion coefficient (D) of oxygen in lead divided by the boundary layer thickness (δ), around the bubble, and D is a function of temperature. The bold lines represent Baird and Davidson equation[15] and Lochiel and Calderbank equation[8] in which the values of D for the three temperatures have been taken from the work of Rapp et al[48]. It is seen that the observed increase is somewhat larger. This could be attributed to the uncertainty in the boundary layer thickness δ. It is not known whether δ will also be a function of temperature.

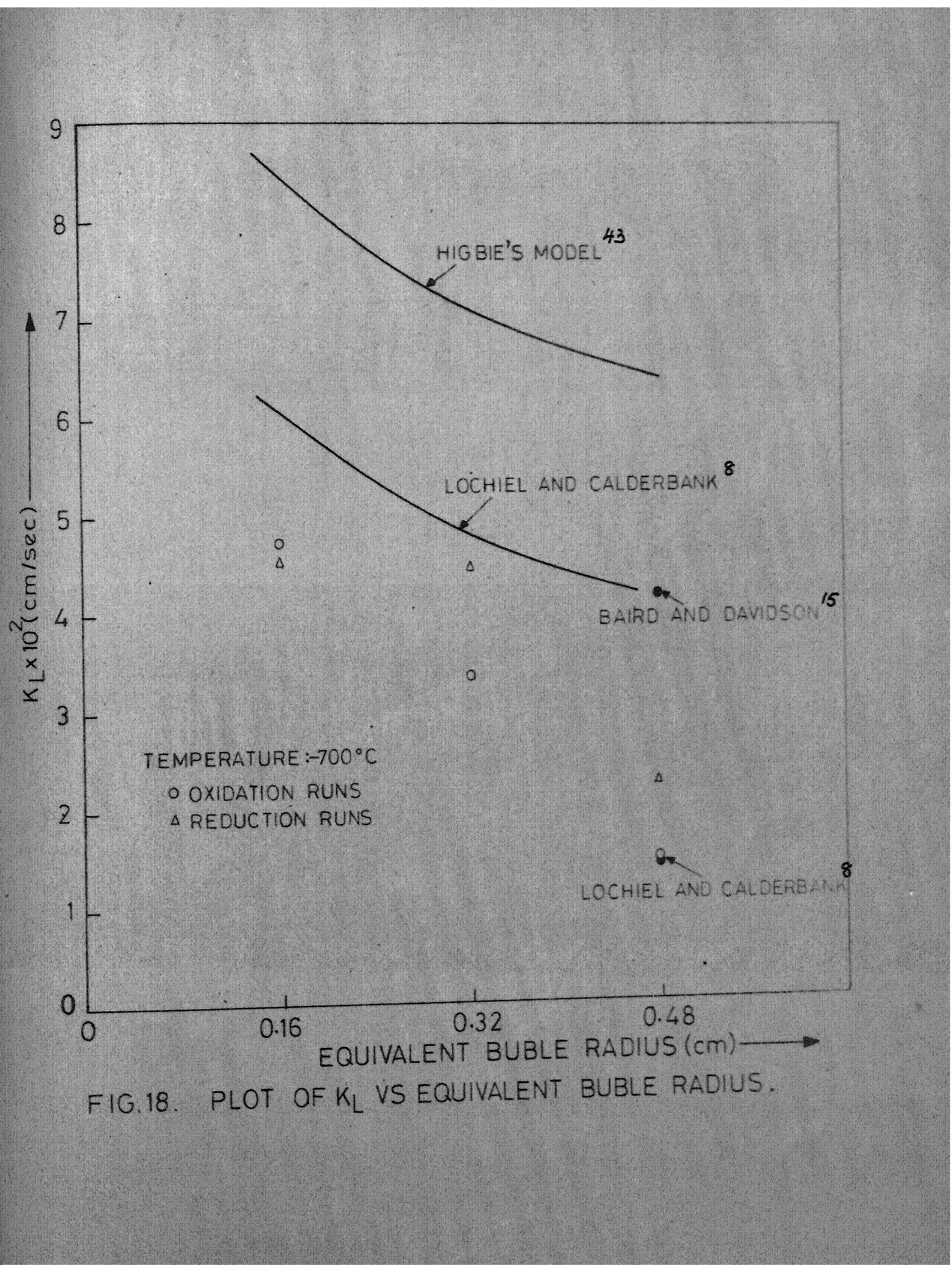


FIG. 18. PLOT OF K_L VS EQUIVALENT BUBLE RADIUS.

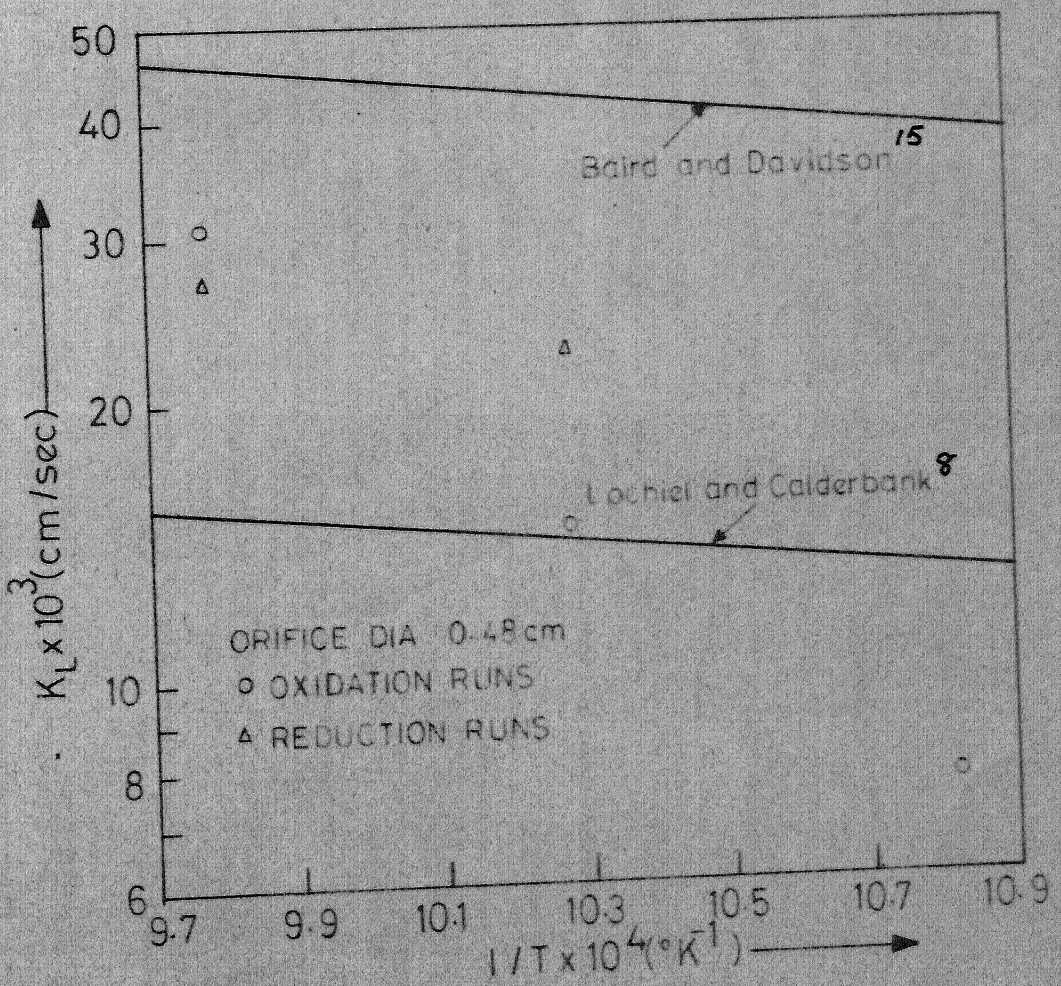


FIG 19. PLOT OF LOG K_L VS $1/T$

TABLE 12

COMPARISON OF OBSERVED VALUES OF K_L WITH THEORETICAL VALUES

Temperature (°C)	Orifice dia. (cm)	Observed K_L (cm/sec)		Theoretical K_L (cm/sec)		
		Oxidation	Reduction	Higbie's Model[43]	Lochiel and Calderbank[8]	Baird and Davidson[15]
700	0.16	0.04709	0.04526	0.08476	0.06059	—
700	0.32	0.03352	0.04455	0.07127	0.04808	—
700	0.48	0.01453	0.02252	—	0.01407	0.04178
650.5	0.48	0.00771	—	—	0.01291	0.03870
750	0.48	0.03073	0.02681	—	0.01522	0.04519

CHAPTER 5

CONCLUSIONS

The main conclusions of the present investigation are summarized below:

1. The phenomena of oxygen transfer during the interaction of a reducing or oxidising bubble with a liquid metal may be successfully studied using an oxide solid-electrolyte cell. The mass transfer phenomena are adequately analysed using equations available in the literature.

2. The rate of transfer of oxygen during either oxidation or reduction is highest for the smallest bubble size and the largest flow rate.

3. The mass transfer coefficient of oxygen in liquid lead (K_L) increases with an increase in temperature for the same bubble size. For the same temperature, it increases with a decrease in bubble size.

4. No conclusion can be drawn on the mass transfer coefficient of oxygen in lead (D/δ) across the free surface of the liquid lead because of the uncertainty of the surface.

CHAPTER 6

SUGGESTIONS FOR FURTHER STUDIES

The solid-electrolyte cell technique offers a quick and reliable means of studying the kinetics of oxidation and deoxidation. Any number of liquid metals can be studied in a similar manner as lead has been studied in this work. However, in this work, the geometry used entails a large wall effect on the rising bubble. Further studies could be performed with a larger container for the liquid metal.

Another possible study can be the effect of impurities in a liquid metal on the kinetics of its oxidation or reduction. Moreover the preferential oxidation of an element or even a number of elements in a basis metal can be investigated.

Upon studying a sufficient number of bubble-metal systems an attempt can be made to formulate a correlation which will express the mass transfer coefficient K_L in terms of the properties of the liquid metal and the dimensions of the bubble.

LIST OF REFERENCES

1. Dutta, R.L., Napier, D.H. and Howitt, D.M. - Trans. Instn. Chem. Engrs. 28, (1950), 14.

2. Peebles, F.N. and Garber, H.J. - Chem. Engg. Prog., 49 (1953), 88.

3. Haberman, W.L. and Morton, R.K. - David Taylor Model Basin Rep. No. 802 (1953).

4. Hadamard, J. - C.R. Seanc. Acad. Sci., Paris, 152, (1911), 40.

5. Rybczynski, W. - Bull. Inst. Acad. Sec. Cracovie (A) (1911), 40.

6. Levich, V.G. - 'Physico Chemical Hydrodynamics', Prentice Hall, Englewood Cliffs (1962), Ch. 8.

7. Calderbank, P.H. and Lochiel, A.C. - Chem. Engg. Sci. 19 (1964), 485.

8. Lochiel, A.C. and Calderbank, P.H. - Chem. Eng. Sci. 19 (1964), 471.

9. Davies, R.M. and Taylor, G. - Proc. Roy. Soc. 200A (1950), 375.

10. Collins, R. - Chem. Eng. Sci. 22 (1967), 89.

11. Uno, S. and Kintner, R.C. - A.I.Ch.E. Jl. 2 (1956), 420.

12. Harmerton, D. and Garner, F.H. - Trans. Inst. Chem. Engrs. 32 (1954), 318.

13. Frossling, N. - Beitr. Geophys. 52 (1938), 170.

14. Hughmark, G.A. - Ind. Eng. Chem. Process Des. and Dev. 6 (1967), 218.

15. Baird, M.H.I. and Davidson, J.F. - Chem. Eng. Sci. 17 (1962), 87.

16. Calderbank, P.H. - Trans. Inst. Chem. Engr. 34 (1959), 173; 212 (1967), 209; 36 (1958), 443.

17. Wasilo, S. and Gal-or, B. - Chem. Eng. Sci. 26, (1971), 829.

18. Gal-or, B. and Wasilo, S. - Chem. Eng. Sci. 23 (1968), 1431.

19. Pehlke, R.D. and Bennett, A.L. - Trans. TMS. AIME, 224 (1962), 1237.

20. Bandyopadhyay, G.K. and Ray, H.S. - Met. Trans. 2 (1971), 3055; Bandyopadhyay, G.K. - 'Kinetics of oxidation and deoxidation of molten lead', M.Tech. Thesis, Dept. of Met. Engg., IIT-Kanpur (1970).

21. Nanda, C.R. and Geiger, G.H. - Met. Trans. 2 (1971), 1101.

22. Jackson, R.W. - Ind. Chem. 28 (1952), 346.

23. Leibson, I., Holcomb, E.G., Cacoso, A.G., and Jacmic, J.J.- A.I.Ch.E.Jl. 2 (1956), 296.

24. Papamentellos, D., Lange, K.W., Okohira, K., and Schenck, H.- Met. Trans. 2, (1971), 3135.

25. Davenport, W.G., Bradshaw, A.V., and Richardson, F.D. - J. Iron and Steel Inst. 205 (1967), 1034.

26. Panenis M. and Davenport, W.G. - Trans. TMS. AIME 245 (1969), 735.

27. Guthrie, R.I.L. and Bradshaw, A.V. - Trans. TMS. AIME 245 (1969), 2285.

28. Wagner, G. - J. Phys. Chem. 21 (1963), 1819.

29. Schmalzried, H. and Trojakow, J.D. - Z. Electrochem. (1966), 180.

30. Tare, V.B. and Schmalzried, H. - Trans. TMS. AIME. 236 (1966), 444.

31. Masson, C.R. and Whiteway, S.G. - Canadian Met. Quart. 6 (1966), 199.

32. Rickert, H. and Steiner, R. - Z. Phys. Chem. 49 (1966), 127.

33. Rapp, R.A. in 'Proceeding, Conference on Thermodynamics of Nuclear Materials', Vienna, 1967. (Int. At. Energy, Agency, Vienna, 1968, 559.)

34. Belton, G.R., 'The diffusivity of oxygen in liquid lead by a steady state electrolyte cell technique', paper presented at the annual meeting of the AIME, Feb. 1969, Ab, J.of Metals 20 (1968). December.

35. Ratchford, H. and Rickert, H. - Z. Electrochem. 66 (1962), 497.

36. Birks, N. and Rickert, H. - ibid, 67 (1963), 97.

37. Rickert, H. - ibid 65 (1961), 463.

38. Birks, N. and Rickert, H. - ibid 67 (1963), 501.

39. Goto, K. and Matsushita, Y. - Tetsu-to-Hagane 50 (1964), 1818.

40. Goto, K., Someno, M., Sano, H., and Nagata, K. - Met. Trans. 1 (1970), 23.

41. Alcock, C.B. and Belford, T.N. - Trans. Far. Soc. 60 (1964), 822.

42. Themelis, N.J. and Schmidt, P.R. - Internal Report No. 64, Department of Chemical Engineering, Noranda Research Centre, Quebec.

43. Higbie, R. - Trans. A.I.Ch.E. 31 (1935), 365.

44. Steele, D.C.H. and Alcock, C.B. - Trans. TMS. AIME 233 (1965), 1359.

45. Richardson, F.D. - Trans. TMS. AIME, 230 (1964), 1221.

46. Johnson, A.J., Besik., F., and Hamilton, A.E. - Can. J. Chem. Eng. 47 (1969), 559.

47. McCabe, W.L. and Smith, J.C. - 'Unit operations of chemical engineering', McGraw-Hill Book Co., Kogakusha Co. Ltd., Tokyo (1967), 168.

48. Saware, R., Oberg, K.E., and Rapp, R.A. - The Diffusivity and Solubility of Oxygen in Liquid Lead from Electrochemical Measurements. High Temperature Electrochemical Research in Metallurgy. Fourth Semi-Annual Report. Ohio State University. Dec. 1971.

49. Handbook of Chemistry and Physics. Ed. C.D. Hodgman. The Chemical Rubber Publishing Co. (1961).